

Sensing-Then-Beamforming: Robust Transmission Design for RIS-Empowered Integrated Sensing and Covert Communication

Xingyu Zhao, Min Li, *Member, IEEE*, Ming-Min Zhao, *Senior Member, IEEE*, Shihao Yan, *Senior Member, IEEE*, and Min-Jian Zhao, *Member, IEEE*

Abstract—Traditional covert communication often relies on the knowledge of the warden’s channel state information, which is inherently challenging to obtain due to the non-cooperative nature and potential mobility of the warden. The integration of sensing and communication technology provides a promising solution by enabling the legitimate transmitter to sense and track the warden, thereby enhancing transmission covertness. In this paper, we develop a framework for sensing-then-beamforming in reconfigurable intelligent surface (RIS)-empowered integrated sensing and covert communication (ISCC) systems, where the transmitter (Alice) estimates and tracks the mobile aerial warden’s channel using sensing echo signals while simultaneously sending covert information to multiple legitimate users (Bobs) with the assistance of RIS, under the surveillance of the warden (Willie). Considering channel estimation errors, we formulate a robust non-convex optimization problem that jointly designs the communication beamformers, the sensing signal covariance matrix at Alice, and the phase shifts at the RIS to maximize the covert sum rate of Bobs while satisfying the constraints related to covert communication, sensing, transmitter power, and the unit modulus of the RIS elements. To solve this complex problem, we develop an efficient algorithm using alternating optimization, successive convex approximation, S-procedure, sequential rank-one constraint relaxation, and semidefinite relaxation techniques. Numerical results confirm the convergence of the proposed algorithm and demonstrate its effectiveness in tracking the warden’s channel while ensuring robust covert transmission. Furthermore, the results highlight the advantages of using RIS to enhance the covert transmission rate compared to baseline schemes, and also illustrate the intricate trade-off between communication and sensing in ISCC systems.

Index Terms—Robust transmission design, reconfigurable intelligent surface, integrated sensing and covert communication systems.

I. INTRODUCTION

Covert communication has gained significant attention for its superior protection capabilities compared to traditional physical layer security (PLS), aiming to prevent the wardens from detecting legitimate transmission from received signals [1]. Concurrently, the reconfigurable intelligent surface (RIS) is emerging as a promising technique to enhance spectral and energy efficiency in future wireless communication systems through dynamically reconfiguring wireless channels by precisely controlling the phase shifts of its passive reflecting elements [2]. It has the capability to effectively enhance covert

communication performance [1]. However, traditional covert communication often assumes prior knowledge of wardens’ channel state information (CSI) [3]–[11], which is unrealistic due to the non-cooperative nature between the legitimate transmitter and the wardens. Therefore, finding effective methods to obtain relevant CSI on wardens for covert communication is crucial.

Integrated Sensing and Communications (ISAC) provides a promising solution for traditional covert communication by enabling the legitimate transmitter to sense and track the wardens [1]. In contrast to independent sensing and communication systems, ISAC systems can improve spectrum utilization and reduce equipment size by sharing the same frequency band and hardware for both functionalities [12], [13]. Therefore, the inherent and complementary advantages of covert communication, RIS, and ISAC position the RIS-empowered Integrated Sensing and Covert Communications (ISCC) as a promising technology for both civil and military applications. This technology ensures that communication information, embedded into the sensing waveform and transmitted with assistance from RIS, avoids interception by wardens during sensing tasks [1], [14]. However, fully leveraging the sensing capability to assist in the transmission design for ISCC systems remains an open problem, particularly when coupled with the optimization of RIS configuration.

A. Prior Works and Motivations

There have been growing research interests in covert communication from various perspectives in recent years. In particular, [3] developed both covert beamformer design and low-complexity zero-forcing beamformer design to maximize the covert rate based on the perfect CSI of warden, and then proposed a robust beamforming scheme to handle the imperfect CSI. Furthermore, exploring the combination of RIS with covert communication has tremendous potential to significantly improve system performance [5]–[8]. Specifically, [5] designed a robust beamforming scheme for RIS-empowered Internet of Things (IoT) networks to maximize covert rate. The work [6] proposed the transmit power and the RIS reflection coefficients jointly to enhance the reflection signal at the communication user and deteriorate the detection performance at the warden. By considering the detection error probability constraint at the warden and the communication outage probability of the legitimate user, [7] developed a RIS-empowered multi-antenna covert communications system to improve covert rate. The work [8] studied a RIS-assisted covert transmission scheme with either instantaneous or partial CSI of the warden’s link, which maximizes the covert rate by jointly optimizing the transmit power at Alice and the passive reflection coefficients at the RIS.

X. Zhao, M. Li, M. M. Zhao and M. J. Zhao are with the College of Information Science and Electronic Engineering and the Zhejiang Provincial Key Laboratory of Information Processing, Communication and Networking, Zhejiang University, Hangzhou 310027, China (e-mail: zhaoxingyu23@zju.edu.cn; min.li@zju.edu.cn; zmblack@zju.edu.cn; mjzhao@zju.edu.cn). (*Corresponding author: Min Li.*)

S. Yan is with the School of Science, Edith Cowan University, Perth, WA 6027, Australia (e-mail: s.yan@ecu.edu.au).

Nevertheless, to the best of our knowledge, ISCC amalgamating the strengths of ISAC and covert communication, has not been well investigated. The authors in [9] jointly designed the robust beamformers related to target detection and single-user communication to maximize the radar detection mutual information (or the communication rate) while guaranteeing the covertness requirement for legitimate communication. In [10], a robust beamforming scheme was proposed to maximize the covert throughput subject to covertness and radar detection constraints, which demonstrated the performance trade-off between radar detection and covert communication. The work [11] designed a beamforming framework for RIS-empowered ISCC systems to maximize the communications rate and radar probing power. Additionally, recent work [15] and [16] investigated robust beamforming design under imperfect CSI to achieve a balance among the radar performance, the communication requirements, and the covertness. While the aforementioned works have offered valuable insights into the designs of ISCC systems, they did not address the channel acquisition mechanism concerning the warden and mainly assumed that the instantaneous or statistical CSI of the warden is known.

Benefiting from the design of sensing-assisted communication, recent studies, such as [17] and [18], have leveraged radar sensing to track and jam aerial adversaries while safeguarding legitimate communication. By predicting the corresponding CSI with an extended Kalman filter (EKF) based on backscattered echo signals, [17] proposed a robust resource allocation design for multiple legitimate users to optimize the trade-off between sensing and communication, accounting for channel prediction error and secure communication requirements. However, the approaches and insights presented in [17] are not directly applicable to covert communications, since it focused on secure communication from a physical layer security perspective. In [18], sensing information was used to construct the adversary target's CSI, and the transmit beamforming and radar waveform were designed to maximize the covert transmission rate for a single-user scenario under tracking accuracy constraint. However, it does not explore the scenarios involving multiple legitimate receivers, nor does it investigate further the tradeoff between sensing and covert communication. Moreover, neither [17] nor [18] considers the integration of RIS to enhance transmission capabilities.

B. Contributions and Paper Organization

In this paper, we investigate the robust transmission design for RIS-empowered ISCC systems in the presence of an aerial adversary warden. Due to its exceptional maneuverability and mobility, the warden can pose a significant threat to terrestrial communications. To address this issue, we propose a sensing-then-beamforming framework to enhance the system's robustness and covertness against such aerial adversaries. On the one hand, Alice with dual-functional signals can construct the relevant CSI of the warden Willie by actively sensing and tracking in real-time. On the other hand, considering the channel estimation errors of the warden, a robust transmission design related to the joint optimization of the communication beamformers, the sensing signal covariance matrix at Alice, and the phase shifts at the RIS is proposed to further improve the covert sum rate of Bobs. The main contributions of this paper are as follows:

- For the channel acquisition of Alice-Willie link and RIS-Willie link, we propose a novel sensing-then-

beamforming framework in which Alice utilizes sensing capability to track the trajectory of warden Willie based on the EKF technique and then constructs the corresponding CSI. By considering the imperfect predicted CSI of Willie, we then formulate a robust transmission design problem for multiple legitimate Bobs, aiming to maximize their covert sum rate by jointly designing the communication beamformers, the sensing signal covariance matrix at Alice, and the phase shifts at the RIS, while guaranteeing the constraints related to covert communication, sensing, and the unit-modulus constraints of RIS elements.

- To tackle the challenges posed by the highly non-convex and multivariate optimization problem of the robust transmission design, we first decompose the original non-convex problem into two subproblems, i.e., the design of the communication beamformers and sensing signal covariance matrix at Alice and the design of the phase shifts at the RIS. Subsequently, the successive convex approximation (SCA) method is applied to handle the non-convex objective functions of each subproblem. Based on the S-procedure, we transform the non-convex covert communication constraint containing the dual CSI errors (Alice-Willie link and RIS-Willie link) into a more tractable form. Additionally, by introducing auxiliary variables, the non-convex sensing constraint is converted into an equivalent convex constraint. For the non-convex unit-modulus constraint of RIS, we propose a sequential rank-one constraint relaxation method to handle it. Finally, an alternating optimization (AO) approach is applied to update the Alice transmitter design and the RIS phase-shift design iteratively to achieve a better covert sum rate.
- Simulation results demonstrate that our proposed framework can effectively track the warden's channel while ensuring robust covert transmission. Additionally, the results confirm the effectiveness of our proposed algorithm compared to baseline methods and reveal that deploying RIS significantly improves the covert sum rate of Bobs compared to not deploying RIS at the same level of covertness. Furthermore, we illustrate the trade-off between covert communication and sensing.

The rest of this paper is organized as follows. Section II presents the RIS-empowered ISCC system model. Section III first elaborates the transmission protocol, formulates the robust transmission design problem, and then proposes an efficient algorithm for solving it. Numerical results are provided in Section IV, while the conclusions are drawn in Section V.

Notations: a (or A), \mathbf{a} and \mathbf{A} stand for a scalar, a column vector and a matrix, respectively. The imaginary unit of a complex number is denoted by $j = \sqrt{-1}$. $\mathbb{C}^{m \times n}$ and \mathbb{H}^m denote the sets of all $m \times n$ complex-valued matrices and all $m \times m$ Hermitian matrices, respectively. $(\cdot)^*$, $(\cdot)^T$ and $(\cdot)^H$ respectively represent the conjugate, transpose and conjugate transpose operations of a or \mathbf{A} . $|\cdot|$, $\|\cdot\|$, $\|\cdot\|_F$ and $\Re\{\cdot\}$ denote the determinant (or module for a complex variable), l_2 norm, Frobenius norm, and real part, respectively. $\text{tr}(\cdot)$, $\text{diag}\{\cdot\}$ and $(\cdot)^{-1}$ denote the trace, the diagonal and the matrix inversion operators, respectively. $\text{blkdiag}(\mathbf{X}, \mathbf{Y})$ is a block diagonal matrix whose diagonal components are matrices \mathbf{X} and \mathbf{Y} . \otimes is the Kronecker product and $\mathbf{A} \succeq \mathbf{0}$ means that \mathbf{A} is a symmetric and positive semi-definite (PSD) matrix. \mathbf{I}_N denotes the $N \times N$ identity matrix, while $\mathbf{0}_{N \times M}$ denotes an $N \times M$ all-zero matrix. $\mathbf{x} \sim \mathcal{CN}(\boldsymbol{\mu}, \mathbf{K})$ means that \mathbf{x} is a cir-

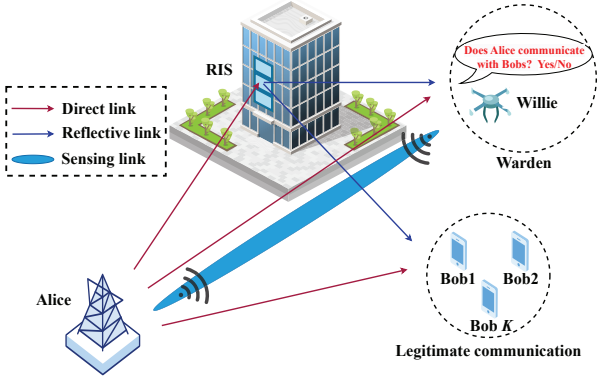


Fig. 1: Illustration of the RIS-empowered ISCC system.

cularly symmetric complex Gaussian vector whose mean and covariance matrix are $\boldsymbol{\mu}$ and \mathbf{K} , respectively. The maximum eigenvalue of matrix \mathbf{A} and the corresponding eigenvector are represented by $\lambda_{\max}(\mathbf{A})$ and $\mathbf{u}_{\max}(\mathbf{A})$. $\nabla_{\mathbf{A}} f$ denotes the gradient of f with respect to matrix \mathbf{A} . Furthermore, \mathcal{O} represents the big-O notation. Finally, $\mathcal{K} \triangleq \{1, \dots, K\}$ and $\mathcal{K}_k \triangleq \mathcal{K} \setminus \{k\}$.

II. SYSTEM MODEL

As shown in Fig. 1, we consider a downlink narrowband RIS-empowered ISCC system, which consists of a dual-functional radar-communication Alice, K single-antenna legitimate users (Bobs), a mobile illegal warden (Willie) with a single antenna, and one RIS. Alice equipped with two rectangular uniform planar arrays (UPAs) performs multi-user covert communication and related sensing tasks to track the trajectory of Willie, such as an adversary unmanned aerial vehicle (UAV), simultaneously. Without loss of generality, the numbers of transmit and receive antennas, denoted by N_A^t and N_A^r , are assumed to be identical, i.e., $N_A^t = N_A^r = N_H N_V = N_A$, where N_H and N_V denote the numbers of antennas in the horizontal and vertical dimensions, respectively. RIS with N_R passive elements is deployed to improve the system performance. Meanwhile, Willie aims to determine whether or not Alice is transmitting signals to Bobs.

A. Signal Model

1) *Communication Signal*: Consider a frame consisting of N time slots. Let T be the frame duration, and thus each time slot occupies $\delta = T/N$ unit time. Then, the received communication signal at Bob k in time slot n is given by

$$y_k(n, t) = \underbrace{\mathbf{h}_k^H[n] \mathbf{w}_k[n] s_k(n, t)}_{\text{desired signal}} + \underbrace{\sum_{j \in \mathcal{K}_k} \mathbf{h}_j^H[n] \mathbf{w}_j[n] s_j(n, t)}_{\text{inter-user interference}} + \underbrace{\mathbf{h}_k^H[n] \mathbf{s}_r(n, t)}_{\text{sensing signal}} + \underbrace{n_k(n, t)}_{\text{noise}}, k \in \mathcal{K}, \quad (1)$$

where $t \in (0, \delta)$ is a time instant within time slot $n \in \{1, \dots, N\}$. $s_k(n, t) \sim \mathcal{CN}(0, 1)$ represents the transmitted information signal to Bob k with the corresponding beamformer $\mathbf{w}_k[n] \in \mathbb{C}^{N_A \times 1}$. The term $\mathbf{s}_r(n, t)$ represents the sensing signal with the same deterministic covariance matrix $\mathbf{R}_s[n] \in \mathbb{C}^{N_A \times N_A}$ for each signal sample in time slot n . In addition, the equivalent channel vector $\mathbf{h}_k^H[n] \triangleq \mathbf{h}_{d,k}^H + \mathbf{h}_{r,k}^H \boldsymbol{\Theta}[n] \mathbf{G}$ is comprised of the Alice-RIS link $\mathbf{G} \in \mathbb{C}^{N_R \times N_A}$, the RIS-Bob k

link $\mathbf{h}_{r,k}^H \in \mathbb{C}^{1 \times N_R}$, and the Alice-Bob k link $\mathbf{h}_{d,k}^H \in \mathbb{C}^{1 \times N_A}$. $\boldsymbol{\Theta}[n] \triangleq \text{diag}\{\boldsymbol{\theta}[n]\}$ with $\boldsymbol{\theta}[n] = [e^{j\theta_1[n]}, \dots, e^{j\theta_{N_R}[n]}]^T$ denotes the RIS phase shift matrix [5], [11]. Considering the coordination nature among legitimate parties and with the help of some advanced channel estimation methods [19], [20], we assume the availability of perfect CSI for all links related to legitimate communication during the whole transmission period. Finally, $n_k(n, t) \sim \mathcal{CN}(0, \sigma_{b,k}^2)$ is the additive white Gaussian noise (AWGN) at Bob k with $\sigma_{b,k}^2$ denoting the noise variance.

2) *Sensing Signal*: In order to transmit and receive signals simultaneously, the full-duplex mode is considered at the transmitter side, so that the received echo signal at Alice reflected by Willie can be expressed as¹ [17], [22]

$$\mathbf{r}_w(n, t) = e^{j2\pi v_w[n]t} \underbrace{\mathbf{H}_{rw}[n] \sum_{k \in \mathcal{K}} \mathbf{w}_k[n] s_k(n, t - \tau_w[n])}_{\text{echo of communication signal}} + e^{j2\pi v_w[n]t} \underbrace{\mathbf{H}_{rw}[n] \mathbf{s}_r(n, t - \tau_w[n])}_{\text{echo of sensing signal}} + \mathbf{n}_r(n, t), \quad (2)$$

where $v_w[n]$ and $\tau_w[n]$ denote the Doppler shift and round-trip time delay, respectively. $\mathbf{n}_r(n, t)$ is the background AWGN with each entry obeying $\mathcal{CN}(0, \sigma_r^2)$. Due to the strong line-of-sight (LoS) nature for an aerial adversary Willie [23], the target response channel matrix $\mathbf{H}_{rw}[n]$ is given by

$$\mathbf{H}_{rw}[n] = \sqrt{\frac{\rho_0 \varsigma}{d_{aw}^4[n]}} \mathbf{a}(\theta_{aw}[n], \phi_{aw}[n]) \mathbf{a}^H(\theta_{aw}[n], \phi_{aw}[n]), \quad (3)$$

where $d_{aw}[n]$ is the distance between Alice and Willie. ρ_0 and ς represent the channel power at the reference distance of one meter and the radar cross-section (RCS) of Willie, respectively. The steering vector $\mathbf{a}(\theta, \phi) \in \mathbb{C}^{N_A \times 1}$ is given by

$$\mathbf{a}(\theta, \phi) = \left[1, e^{j\pi \sin(\phi) \sin(\theta)}, \dots, e^{j\pi(N_H-1) \sin(\phi) \sin(\theta)} \right]^T \otimes \left[1, e^{j\pi \cos(\phi)}, \dots, e^{j\pi(N_V-1) \cos(\phi)} \right]^T, \quad (4)$$

where we assume half-wavelength antenna spacing for UPA, while θ and ϕ represent the azimuth angle of departure (AoD) and the elevation AoD from Alice to Willie, respectively.

B. Tracking Model

Unlike the assumptions in [5], [9], [11] that the perfect/statistical CSI of the Alice-Willie link can be obtained, we consider a more practical scenario where Alice must actively estimate and track the channel of the mobile Willie. Thus, Alice is required to estimate the location of Willie first and thereby construct the channels for the Alice-Willie link and the RIS-Willie link to achieve effective covert transmission. To this end, we employ the EKF technique to track and predict the location of Willie based on the estimated velocity information [17], [24]. In particular, the known and fixed locations of Alice and RIS are denoted as $\mathbf{q}_a = [x_a, y_a, z_a]^T$ and $\mathbf{q}_r = [x_r, y_r, z_r]^T$, respectively. In time slot n , the location

¹Note that we omit the sensing signals reflected by RIS, i.e., the Alice-RIS-Willie-RIS-Alice link signals, which suffer severe product-distance round-trip path-loss over the multiple signal reflections compared to the direct reflected link [21].

of Willie is denoted as $\mathbf{q}_w[n] = [x_w[n], y_w[n], z_w[n]]^T$ and the corresponding speed is $\dot{\mathbf{q}}_w[n] = [\dot{x}_w[n], \dot{y}_w[n], \dot{z}_w[n]]^T$. The state of Willie, i.e., $\chi_w[n] = [\mathbf{q}_w^T[n], \dot{\mathbf{q}}_w^T[n]]^T \in \mathbb{R}^{6 \times 1}$, is unknown to Alice and required to be estimated. The entire modeling and execution process of EKF are elaborated as follows:

1) *State evolution model of Willie*: Considering the non-cooperativity between Alice and Willie, we adopt a simple yet practical constant velocity movement model where the velocity of Willie is assumed to remain unchanged within two adjacent slots. The state evolution model of Willie is then given by

$$\chi_w[n] = \mathbf{F}\chi_w[n-1] + \mathbf{n}_{\chi_w}, \mathbf{F} = \begin{bmatrix} \mathbf{I}_3 & \delta \mathbf{I}_3 \\ \mathbf{0}_3 & \mathbf{I}_3 \end{bmatrix}, \quad (5)$$

where $\mathbf{F} \in \mathbb{R}^{6 \times 6}$ is the state transition matrix, $\mathbf{n}_{\chi_w} \sim \mathcal{N}(\mathbf{0}, \mathbf{Q}_{\chi_w})$ denotes the state evolution noise vector with $\mathbf{Q}_{\chi_w} = \text{diag}\{\sigma_{x_w}^2, \sigma_{y_w}^2, \sigma_{z_w}^2, \sigma_{\dot{x}_w}^2, \sigma_{\dot{y}_w}^2, \sigma_{\dot{z}_w}^2\}$ obtained based on the long-term measurements at Alice [17], [18].

2) *Measurement model of Willie*: We consider the matched-filter (MF) principle and exploit the reflected echo signal to estimate $v_w[n], \tau_w[n], \theta_{aw}[n]$ and $\phi_{aw}[n]$ in (2). According to [17], [24], [25], the estimation error variances of these parameters can be given as

$$\begin{aligned} \sigma_{\tau_w[n]}^2 &= \frac{c_{\tau_w}}{\text{SNR}[n]}, \sigma_{v_w[n]}^2 = \frac{c_{v_w}}{\text{SNR}[n]}, \\ \sigma_{\theta_{aw}[n]}^2 &= \frac{c_{\theta_{aw}}}{\text{SNR}[n]}, \sigma_{\phi_{aw}[n]}^2 = \frac{c_{\phi_{aw}}}{\text{SNR}[n]}, \end{aligned} \quad (6)$$

where $c_{\tau_w}, c_{v_w}, c_{\theta_{aw}}, c_{\phi_{aw}} > 0$ are determined by the adopted estimation methods, and $\text{SNR}[n]$ is the output SNR of the MF given by

$$\begin{aligned} \text{SNR}[n] &= \frac{\rho_{0\varepsilon} G_{\text{MF}} N_A \mathbf{a}^H(\theta_{aw}[n], \phi_{aw}[n]) \mathbf{R}_s[n] \mathbf{a}(\theta_{aw}[n], \phi_{aw}[n])}{\sigma_{\tau_w}^2 d_{aw}^4[n]}, \end{aligned} \quad (7)$$

where G_{MF} is the MF gain related to the number of transmit symbols in a time slot. Then, based on $\chi_w[n]$ and \mathbf{q}_a , the measurement equations associated with $v_w[n], \tau_w[n], \theta_{aw}[n]$, and $\phi_{aw}[n]$ can be established as

$$\begin{cases} \hat{\tau}_w[n] = \frac{2\|\mathbf{q}_w[n] - \mathbf{q}_a\|}{c} + n_{\tau_w}[n], \\ \hat{v}_w[n] = \frac{2\dot{\mathbf{q}}_w^T[n](\mathbf{q}_w[n] - \mathbf{q}_a) f_c}{c\|\mathbf{q}_w[n] - \mathbf{q}_a\|} + n_{v_w}[n], \\ \sin \hat{\theta}_{aw}[n] = \frac{y_w[n] - y_a}{\sqrt{|x_w[n] - x_a|^2 + |y_w[n] - y_a|^2}} + n_{\sin \theta_{aw}[n]}, \\ \cos \hat{\theta}_{aw}[n] = \frac{x_w[n] - x_a}{\sqrt{|x_w[n] - x_a|^2 + |y_w[n] - y_a|^2}} + n_{\cos \theta_{aw}[n]}, \\ \sin \hat{\phi}_{aw}[n] = \frac{z_w[n] - z_a}{\|\mathbf{q}_w[n] - \mathbf{q}_a\|} + n_{\sin \phi_{aw}[n]}, \end{cases} \quad (8)$$

where $f_c = \frac{c}{\lambda_c}$ with c and λ_c denoting the speed of light and wavelength, respectively. $n_{\tau_w}[n], n_{v_w}[n], n_{\sin \theta_{aw}[n]}, n_{\cos \theta_{aw}[n]}$, and $n_{\sin \phi_{aw}[n]}$ denote the corresponding measurement noises and are assumed to follow Gaussian distribution with zero mean and variances $\sigma_{\tau_w}^2[n], \sigma_{v_w}^2[n], \sigma_{\sin \theta_{aw}[n]}^2, \sigma_{\cos \theta_{aw}[n]}^2$ and $\sigma_{\sin \phi_{aw}[n]}^2$, respectively. Similar to [17], [22], we adopt the following approximations: $\sigma_{\sin \theta_{aw}[n]}^2 \approx \cos^2 \hat{\theta}_{aw}[n] \sigma_{\theta_{aw}[n]}^2$, $\sigma_{\cos \theta_{aw}[n]}^2 \approx \sin^2 \hat{\theta}_{aw}[n] \sigma_{\theta_{aw}[n]}^2$ and $\sigma_{\sin \phi_{aw}[n]}^2 \approx \cos^2 \hat{\phi}_{aw}[n] \sigma_{\phi_{aw}[n]}^2$ in the high SNR regime. Furthermore, by defining $\tilde{c}_{\theta_{aw}} \triangleq c_{\theta_{aw}} \cos^2 \hat{\theta}_{aw}^2[n]$ and $\tilde{c}_{\phi_{aw}} \triangleq c_{\phi_{aw}} \cos^2 \hat{\phi}_{aw}^2[n]$ and collecting all measurement parameters in (8), the measurement model of Willie in (8) can be rewritten

as the following more compact form:

$$\mathbf{Z}_w[n] = \mathbf{g}(\chi_w[n]) + \mathbf{n}_{\mathbf{Z}_w[n]}, \quad (9)$$

where

$$\mathbf{Z}_w[n] = [\hat{\tau}_w[n], \hat{v}_w[n], \sin \hat{\theta}_{aw}[n], \cos \hat{\theta}_{aw}[n], \sin \hat{\phi}_{aw}[n]]^T,$$

and the non-linear function $\mathbf{g} : \mathbb{R}^{6 \times 1} \rightarrow \mathbb{R}^{4 \times 1}$ represents the mapping from $\chi_w[n]$ to $\mathbf{Z}_w[n]$. $\mathbf{n}_{\mathbf{Z}_w[n]}$ denotes the zero-mean Gaussian noise vector and its covariance matrix $\hat{\mathbf{Q}}_{\mathbf{Z}_w[n]}$ can be estimated as follows²

$$\begin{aligned} \hat{\mathbf{Q}}_{\mathbf{Z}_w[n]} &= \text{diag}\left\{\sigma_{\tau_w}^2, \sigma_{v_w}^2, \sigma_{\sin \theta_{aw}}^2, \sigma_{\cos \theta_{aw}}^2, \sigma_{\sin \phi_{aw}}^2\right\} \\ &= \frac{\text{diag}\{\tilde{\mathbf{z}}\}}{\mathbf{a}^H(\hat{\theta}_{aw}[n], \hat{\phi}_{aw}[n]) \mathbf{R}_s[n] \mathbf{a}(\hat{\theta}_{aw}[n], \hat{\phi}_{aw}[n])}, \end{aligned} \quad (10)$$

where $\tilde{\mathbf{z}} = \frac{\sigma_{\tau_w}^2 d_{aw}^4[n]}{\rho_{0\varepsilon} G_{\text{MF}} N_A} [c_{\tau_w}, c_{v_w}, \tilde{c}_{\theta_{aw}}, c_{\theta_{aw}} - \tilde{c}_{\theta_{aw}}, \tilde{c}_{\phi_{aw}}]$.

Finally, according to the EKF method, we can linearize the nonlinear measurement model in (9) as

$$\begin{aligned} \hat{\mathbf{Z}}_w[n] &\approx \mathbf{g}(\hat{\chi}_w[n|n-1]) + \mathbf{J}_n(\chi_w[n] - \hat{\chi}_w[n|n-1]) + \mathbf{n}_{\mathbf{Z}_w[n]}, \end{aligned} \quad (12)$$

where $\hat{\chi}_w[n|n-1]$ is the predicted state of Willie in time slot

n . $\mathbf{J}_n = \left. \frac{\partial \mathbf{g}}{\partial \chi_w} \right|_{\chi_w = \hat{\chi}_w[n|n-1]}$ is the Jacobian matrix of \mathbf{g} with $\frac{\partial \mathbf{g}}{\partial \chi_w}$ calculated in (11) on the top of the next page, where

$$\frac{\partial v_e}{\partial x_w} = \frac{2f_c \left(\dot{x}_w \|\mathbf{q}_w - \mathbf{q}_a\|^2 - \dot{\mathbf{q}}_w^T(\mathbf{q}_w - \mathbf{q}_a)(x_w - x_a) \right)}{c \|\mathbf{q}_w - \mathbf{q}_a\|^3},$$

$$\frac{\partial v_e}{\partial y_w} = \frac{2f_c \left(\dot{y}_w \|\mathbf{q}_w - \mathbf{q}_a\|^2 - \dot{\mathbf{q}}_w^T(\mathbf{q}_w - \mathbf{q}_a)(y_w - y_a) \right)}{c \|\mathbf{q}_w - \mathbf{q}_a\|^3},$$

$$\frac{\partial v_e}{\partial z_w} = \frac{2f_c \left(\dot{z}_w \|\mathbf{q}_w - \mathbf{q}_a\|^2 - \dot{\mathbf{q}}_w^T(\mathbf{q}_w - \mathbf{q}_a)(z_w - z_a) \right)}{c \|\mathbf{q}_w - \mathbf{q}_a\|^3},$$

$$\|\mathbf{q}_{ew}\| = \sqrt{(x_w - x_a)^2 + (y_w - y_a)^2}.$$

3) *EKF process*: Based on (5) and (12), the whole process of EKF can be specifically presented as below:

- *Predict the state of Willie* $\hat{\chi}_w[n|n-1]$:

$$\hat{\chi}_w[n|n-1] = \mathbf{F}\hat{\chi}_w[n-1], \quad (13)$$

where $\hat{\chi}_w[n-1]$ is the estimated state of Willie in time slot $n-1$.

- *Predict the covariance matrix* $\mathbf{C}[n|n-1]$:

$$\mathbf{C}[n|n-1] = \mathbf{F}\mathbf{C}[n-1]\mathbf{F}^T + \mathbf{Q}_{\chi_w}. \quad (14)$$

- *Calculate the Kalman gain matrix* \mathbf{K}_n :

$$\mathbf{K}_n = \mathbf{C}[n|n-1] \mathbf{J}_n^T \left(\mathbf{J}_n \mathbf{C}[n|n-1] \mathbf{J}_n^T + \hat{\mathbf{Q}}_{\mathbf{Z}_w[n]} \right)^{-1}. \quad (15)$$

- *Update the corresponding posterior covariance matrix* $\mathbf{C}[n]$:

$$\mathbf{C}[n] = (\mathbf{I}_6 - \mathbf{K}_n \mathbf{J}_n) \mathbf{C}[n|n-1]. \quad (16)$$

²Note that due to the inability to obtain the true angle information about Willie, we have to resort to the related predicted values, that is to say we can only calculate the estimated $\hat{\theta}_{aw}[n]$ and $\hat{\phi}_{aw}[n]$ by using the predicted state $\hat{\chi}_w[n|n-1]$.

$$\frac{\partial \mathbf{g}}{\partial \boldsymbol{\chi}_w} = \begin{bmatrix} \frac{2(x_w - x_a)}{c \|\mathbf{q}_w - \mathbf{q}_a\|} & \frac{2(y_w - y_a)}{c \|\mathbf{q}_w - \mathbf{q}_a\|} & \frac{2(z_w - z_a)}{c \|\mathbf{q}_w - \mathbf{q}_a\|} & 0 & 0 & 0 \\ -\frac{\partial v_w}{\partial x_w} & \frac{\partial v_w}{\partial y_w} & \frac{\partial v_w}{\partial z_w} & \frac{2f_c(x_w - x_a)}{c \|\mathbf{q}_w - \mathbf{q}_a\|} & \frac{2f_c(y_w - y_a)}{c \|\mathbf{q}_w - \mathbf{q}_a\|} & \frac{2f_c(z_w - z_a)}{c \|\mathbf{q}_w - \mathbf{q}_a\|} \\ -\frac{(y_w - y_a)(x_w - x_a)}{\|\mathbf{q}_{ew}\|^3} & \frac{(x_w - x_a)^2}{\|\mathbf{q}_{ew}\|^3} & 0 & 0 & 0 & 0 \\ \frac{(y_w - y_a)^2}{\|\mathbf{q}_{ew}\|^3} & -\frac{(x_w - x_a)(y_w - y_a)}{\|\mathbf{q}_{ew}\|^3} & 0 & 0 & 0 & 0 \\ -\frac{(z_w - z_a)(x_w - x_a)}{\|\mathbf{q}_w - \mathbf{q}_a\|^3} & -\frac{(z_w - z_a)(y_w - y_a)}{\|\mathbf{q}_w - \mathbf{q}_a\|^3} & \frac{\|\mathbf{q}_{ew}\|^2}{\|\mathbf{q}_w - \mathbf{q}_a\|^3} & 0 & 0 & 0 \end{bmatrix} \quad (11)$$

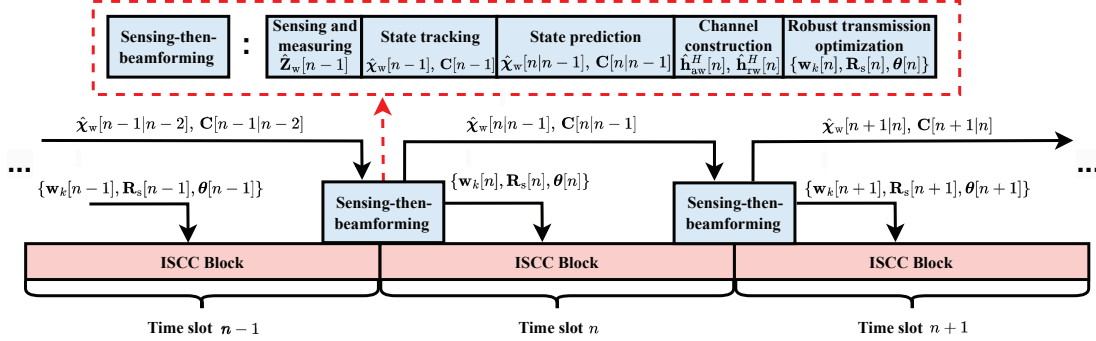


Fig. 2: Diagram of the transmission protocol of RIS-empowered ISCC systems.

- Estimate the state of Willie $\hat{\boldsymbol{\chi}}_w[n]$:

$$\hat{\boldsymbol{\chi}}_w[n] = \hat{\boldsymbol{\chi}}_w[n|n-1] + \mathbf{K}_n \left(\hat{\mathbf{Z}}_w[n] - \mathbf{J}_n (\hat{\boldsymbol{\chi}}_w[n|n-1]) \right). \quad (17)$$

C. Performance Metrics

Based on the aforementioned signal and tracking models, we define the following performance metrics for the considered RIS-empowered ISCC system.

1) *Communication*: According to (1), the covert sum rate of Bobs in time slot n can be expressed as

$$\sum_{k \in \mathcal{K}} R_k[n] = \sum_{k \in \mathcal{K}} \log_2(1 + \text{SINR}_k), \quad (18)$$

where the signal-to-interference-plus-noise ratio (SINR) of Bob k is

$$\text{SINR}_k = \frac{|\mathbf{h}_k^H[n] \mathbf{w}_k[n]|^2}{\sum_{j \in \mathcal{K}_k} |\mathbf{h}_k^H[n] \mathbf{w}_j[n]|^2 + \mathbf{h}_k^H[n] \mathbf{R}_s[n] \mathbf{h}_k[n] + \sigma_{b,k}^2}. \quad (19)$$

2) *Sensing*: By substituting (15) into (16), we have

$$\mathbf{C}[n] = \left(\mathbf{C}^{-1}[n|n-1] + \mathbf{J}_n^T \hat{\mathbf{Q}}_{\mathbf{z}_w[n]}^{-1} \mathbf{J}_n \right)^{-1}. \quad (20)$$

Note that $\text{tr}(\mathbf{C}[n])$ characterizes the posterior mean square error (MSE) for tracking the state of Willie, which means that limiting the value of $\text{tr}(\mathbf{C}[n])$ to a target threshold, e.g., MSE_{\max} , can effectively ensure certain sensing accuracy, i.e.,

$$\text{tr}(\mathbf{C}[n]) \leq \text{MSE}_{\max}. \quad (21)$$

3) *Covertiness*: In our considered system, the focus is on protecting the intention behind transmitting information signals. Therefore, Willie conducts a binary hypothesis test on his received signals in each time slot to determine whether or not Alice is communicating with Bobs. Specifically, considering that each time slot contains L symbols, we denote the received signal of Willie in time slot n as $\mathbf{y}_w[n] = [y_w[n, 1], y_w[n, 2], \dots, y_w[n, L]] \in \mathbb{C}^{1 \times L}$ and then the hypothesis test on $\mathbf{y}_w[n]$ can be written as

$$\mathbf{y}_w[n] = \begin{cases} \mathbf{h}_w^H[n] \mathbf{S}_r[n] + \mathbf{n}_w[n], & \mathcal{H}_0, \\ \mathbf{h}_w^H[n] (\mathbf{W}_c[n] \mathbf{S}_c[n] + \mathbf{S}_r[n]) + \mathbf{n}_w[n], & \mathcal{H}_1, \end{cases} \quad (22)$$

Here, $\mathbf{h}_w^H[n] \triangleq \mathbf{h}_{aw}^H[n] + \mathbf{h}_{rw}^H[n] \boldsymbol{\Theta}[n] \mathbf{G}$, the Alice-Willie link \mathbf{h}_{aw} and RIS-Willie \mathbf{h}_{rw} link can be modeled as ³

$$\mathbf{h}_{iw}^H[n] = \sqrt{\frac{\rho_0}{d_{iw}^2[n]}} \mathbf{a}^H(\theta_{iw}[n], \phi_{iw}[n]), \quad \forall i \in \{a, r\} \quad (23)$$

where $d_{iw}[n]$, $\theta_{iw}[n]$, and ϕ_{iw} , $\forall i \in \{a, r\}$ denote the distance between Alice/RIS and Willie, the azimuth AoD, and the elevation AoD from Alice/RIS to Willie, respectively. $\mathbf{W}_c[n] \triangleq [\mathbf{w}_1[n], \dots, \mathbf{w}_K[n]]$. $\mathbf{S}_c[n] \triangleq [\mathbf{s}_c[n, 1], \dots, \mathbf{s}_c[n, L]] \in \mathbb{C}^{K \times L}$ denotes the communication symbol matrix with i.i.d. elements $\sim \mathcal{CN}(0, 1)$, and each column $\mathbf{s}_c[n, l] = [s_1[n, l], \dots, s_K[n, l]]^T$ with $l \in \{1, \dots, L\}$ is the concatenation of each legitimate Bob's l -th symbol. $\mathbf{S}_r[n] \triangleq [\mathbf{s}_r[n, 1], \dots, \mathbf{s}_r[n, L]] \in \mathbb{C}^{N_A \times L}$ represents the sensing symbol matrix, and each symbol satisfies

$$\mathbb{E} \{ \mathbf{s}_r[n, l] \mathbf{s}_r[n, l]^H \} = \mathbf{R}_s[n] \succeq \mathbf{0}, \forall l. \quad (24)$$

Finally, $\mathbf{n}_w[n] \triangleq [n_w[n, 1], \dots, n_w[n, L]]$ (with i.i.d. elements $\sim \mathcal{CN}(0, \sigma_w^2)$) denotes the noise at Willie.

Given $\mathbf{y}_w[n]$, Willie makes a binary decision (\mathcal{D}_1 or \mathcal{D}_0) that infers whether or not the communication between Alice and Bobs is present in form of (22). Assuming an equal prior probability for \mathcal{H}_0 and \mathcal{H}_1 as in [29], the sum of detection error probabilities can be expressed as $\xi = \Pr(\mathcal{D}_1|\mathcal{H}_0) + \Pr(\mathcal{D}_0|\mathcal{H}_1)$, where $\Pr(\mathcal{D}_1|\mathcal{H}_0)$ and $\Pr(\mathcal{D}_0|\mathcal{H}_1)$ denote the false alarm probability and the missed detection probability, respectively. By using an optimal detector with the minimum detection error probability ξ^* at Willie, the covertness constraint can be written as $\xi^* \geq 1 - \varepsilon$ for a required covertness level $\varepsilon > 0$. However, due to the intractability of ξ^* , we instead lower-bound it via the Pinsker's inequality [9], [29] as $\xi^* \geq 1 - \sqrt{\frac{D(\mathbb{P}_0 \parallel \mathbb{P}_1)}{2}}$, where \mathbb{P}_0 and \mathbb{P}_1 are the probability distributions of $\mathbf{y}_w[n]$ under \mathcal{H}_0 and \mathcal{H}_1 , respectively.

Based on the construction of $\mathbf{y}_w[n]$ in (22), and the assumptions that $\mathbf{W}_c[n]$ is fixed for the n -th slot and each sensing

³Usually, LoS propagation dominates the air-ground links according to the air-ground channel properties. Thus, similar to [17], [26]–[28], adopting a LoS channel model for the link between the Alice/RIS deployed on the ground and Willie in the air is a reasonable approximation. This is particularly valid in rural areas where there is minimal blockage and scattering or when Willie operates at a sufficiently high altitude [23].

symbol satisfies (24), $y_w[n, l], \forall l = 1, \dots, L$ are independently identical distributed. Therefore, we have

$$\begin{aligned} \mathbb{P}_0 &= \mathbb{P}(\mathbf{y}_w[n]|\mathcal{H}_0) = \frac{1}{(\pi\lambda_0)^L} \exp\left(-\frac{|\mathbf{y}_w[n]|^2}{\lambda_0}\right), \\ \mathbb{P}_1 &= \mathbb{P}(\mathbf{y}_w[n]|\mathcal{H}_1) = \frac{1}{(\pi\lambda_1)^L} \exp\left(-\frac{|\mathbf{y}_w[n]|^2}{\lambda_1}\right), \end{aligned} \quad (25)$$

where $\lambda_0 \triangleq \mathbf{h}_w^H[n]\mathbf{R}_s[n]\mathbf{h}_w[n] + \sigma_w^2$ and $\lambda_1 \triangleq \mathbf{h}_w^H[n](\mathbf{R}_s[n] + \mathbf{W}_c[n]\mathbf{W}_c^H[n])\mathbf{h}_w[n] + \sigma_w^2$.

Then, the relative entropy $D(\mathbb{P}_0||\mathbb{P}_1)$ of \mathbb{P}_0 to \mathbb{P}_1 can be quantified as [29], [30]

$$D(\mathbb{P}_0||\mathbb{P}_1) = \int_{-\infty}^{+\infty} \mathbb{P}_0 \ln \frac{\mathbb{P}_0}{\mathbb{P}_1} dy = L \left(\ln \frac{\lambda_1}{\lambda_0} + \frac{\lambda_0}{\lambda_1} - 1 \right), \quad (26)$$

and the covertness constraint $D(\mathbb{P}_0||\mathbb{P}_1) \leq 2\varepsilon^2$ is thus enforced in order to achieve covert communication at any given covertness level $\varepsilon > 0$. Note that perfect knowledge of \mathbf{h}_{aw} and \mathbf{h}_{rw} in (26) is not available in practice. To address this issue, Alice will actively sense and track Willie's location, as detailed in Section II-B, to obtain the estimates of \mathbf{h}_{aw} and \mathbf{h}_{rw} . In the next section, we will formulate a robust covert transmission design that accounts for the estimation errors.

III. ROBUST TRANSMISSION DESIGN BASED ON THE SENSING-THEN-BEAMFORMING FRAMEWORK

In this section, we first elaborate the transmission protocol of the considered RIS-empowered ISCC system, followed by the sensing-then-beamforming framework, and then proceed to design the robust transmission scheme.

A. Transmission Protocol

As shown in Fig. 2, Alice can first send the sensing signal $s_r(n, t)$ and then obtain the measurement values $\hat{\mathbf{Z}}_w[n-1]$ based on the echo signal in (2). Combining $\hat{\mathbf{Z}}_w[n-1]$ with the prior obtained $\hat{\chi}_w[n-1|n-2]$ and $\mathbf{C}[n-1|n-2]$, we can correct the final estimated state $\hat{\chi}_w[n-1]$ and posterior covariance matrix $\mathbf{C}[n-1]$ according to (17) in time slot $n-1$.

Then, based on the first-order Markov process for modeling the movement of Willie in (13), Alice can obtain the predicted state $\hat{\chi}_w[n|n-1]$ and construct the Alice-Willie link $\hat{\mathbf{h}}_{aw}^H[n]$ and RIS-Willie link $\hat{\mathbf{h}}_{rw}^H[n]$ in time slot n by replacing $d_{iw}[n]$, $\theta_{iw}[n]$, and $\phi_{iw}[n]$ in (23) with the corresponding predicted values $\hat{d}_{iw}[n|n-1]$, $\hat{\theta}_{iw}[n|n-1]$, and $\hat{\phi}_{iw}[n|n-1]$, respectively, which are given by

$$\begin{aligned} \hat{d}_{iw}[n|n-1] &= \|\hat{\mathbf{q}}_w[n|n-1] - \mathbf{q}_i\|, \\ \hat{\phi}_{iw}[n|n-1] &= \sin^{-1} \left(\frac{\hat{z}_w[n|n-1] - z_i}{\hat{d}_{iw}[n|n-1]} \right), \\ \hat{\theta}_{iw}[n|n-1] &= \\ \sin^{-1} \left(\frac{\hat{y}_w[n|n-1] - y_i}{\sqrt{|\hat{x}_w[n|n-1] - x_i|^2 + |\hat{y}_w[n|n-1] - y_i|^2}} \right), \end{aligned} \quad \forall i \in \{\mathbf{a}, \mathbf{r}\}. \quad (27)$$

However, due to the inability to accurately determine the true position of Willie, the EKF method itself will introduce estimation errors and the real channels $\mathbf{h}_{aw}^H[n]$ and $\mathbf{h}_{rw}^H[n]$ can be modeled as [5], [17]

$$\mathbf{h}_{aw}^H[n] = \hat{\mathbf{h}}_{aw}^H[n] + \Delta_{aw}[n], \mathbf{h}_{rw}^H[n] = \hat{\mathbf{h}}_{rw}^H[n] + \Delta_{rw}[n], \quad (28)$$

where we characterize the channel estimation errors as follows

$$\begin{aligned} \mathcal{U}_{aw}[n] &\triangleq \left\{ \Delta_{aw}[n] \|\Delta_{aw}[n]\|_2 \leq \delta_{aw}^2[n] \right\}, \\ \mathcal{U}_{rw}[n] &\triangleq \left\{ \Delta_{rw}[n] \|\Delta_{rw}[n]\|_2 \leq \delta_{rw}^2[n] \right\}. \end{aligned} \quad (29)$$

Note that $\delta_{aw}[n]$ and $\delta_{rw}[n]$ represent the upper bounds of the corresponding CSI errors related to the tracking MSE of Willie and is given by

$$\delta_{aw}^2[n] = \|\gamma_{aw}^H \mathbf{C}[n|n-1]\|^2, \delta_{rw}^2[n] = \|\gamma_{rw}^H \mathbf{C}[n|n-1]\|^2 \quad (30)$$

where parameters $\gamma_{aw} \in \mathbb{R}^{6 \times 1}$ and $\gamma_{rw} \in \mathbb{R}^{6 \times 1}$ can be obtained via Monte Carlo simulation as in [31].

Subsequently, by considering the channel estimation errors in (28), Alice can optimize the robust transmission strategy to simultaneously execute integrated sensing and covert communication operations within the ISCC architecture.

Finally, by exploiting the echo signal in time slot n , the new measurements $\hat{\mathbf{Z}}_w[n]$ are taken and the estimated state $\hat{\chi}_w[n]$ is calculated, which also serve as the input in the next time slot to predict the new state of Willie.

B. Problem Formulation

Based on the predicted channels and considering the channel estimation errors in (28), we focus on the robust transmission design that jointly optimizes the communication beamformers and sensing signal covariance matrix at Alice and the phase shifts at the RIS to maximize the covert sum rate of Bobs while satisfying the constraints on covert communication, sensing, transmit power, and unit modulus of the RIS reflection coefficients. Specifically, for covert communication provisioning, we make a worst-case assumption regarding the covertness requirement of Willie and therefore the robust optimization problem in time slot n can be formulated as

$$\begin{aligned} \mathcal{P}_1 : \quad & \max_{\boldsymbol{\theta}[n], \mathbf{R}_s[n], \mathbf{w}_k[n]} \sum_{k \in \mathcal{K}} R_k[n] \\ \text{s.t.} \quad & \text{C1: } \text{tr} \left(\sum_{k \in \mathcal{K}} \mathbf{w}_k[n] \mathbf{w}_k^H[n] + \mathbf{R}_s[n] \right) \leq P_t, \\ & \text{C2: } \max_{\substack{\Delta_{aw}[n] \in \mathcal{U}_{aw}[n] \\ \Delta_{rw}[n] \in \mathcal{U}_{rw}[n]}} D(\mathbb{P}_0||\mathbb{P}_1) \leq 2\varepsilon^2, \\ & \text{C3: } \text{tr}(\mathbf{C}[n]) \leq \text{MSE}_{\max}, \\ & \text{C4: } |\theta_i[n]|^2 = 1, \quad i \in [1 : N_R], \\ & \text{C5: } \mathbf{R}_s[n] \succeq \mathbf{0}. \end{aligned} \quad (31)$$

Herein, C1 is imposed to ensure that the transmit power of Alice is limited to her maximum power P_t . Based on the channel estimation errors in (28), C2 can guarantee the minimum covertness requirement, where $D(\mathbb{P}_0||\mathbb{P}_1)$ is a function of $\boldsymbol{\theta}[n]$, $\mathbf{R}_s[n]$, and $\mathbf{w}_k[n]$ according to (26). C3 depends on $\mathbf{R}_s[n]$, and it ensures Alice's effective sensing ability for tracking Willie's motion trajectory, which, in turn, affects the channel estimation errors in the next time slot, as detailed in (20) and (30). It is worth noting that the coupling between C2 and C3 is established through \mathbf{R}_s , and this coupling affects the optimal power allocation between sensing and communication. Finally, C4 reflects the unit modulus of the passive elements at the RIS, and C5 is imposed as the covariance matrix $\mathbf{R}_s[n]$ of the sensing signal is a Hermitian PSD matrix.

However, solving \mathcal{P}_1 is quite challenging for the following reasons: 1) the optimization variables are strongly coupled, 2) the continuity of the CSI uncertainty sets $\mathcal{U}_{aw}[n]$ and $\mathcal{U}_{rw}[n]$ in C2 leads to infinitely many non-convex constraints, 3) the sensing constraint in C3 and unit modulus constraints in C4 are non-convex. In the following subsections, we develop an efficient AO-based algorithm to solve \mathcal{P}_1 effectively. For

notational simplicity, we omit the time slot index n in the following subsections. The key step of the AO-based algorithm is to solve each subproblem given the fixed solutions of the other subproblems, thus we first decompose the complicated \mathcal{P}_1 into two subproblems with regard to $\{\mathbf{R}_s, \mathbf{w}_k\}$ and $\{\boldsymbol{\theta}\}$ in what follows.

C. Subproblem With Respect to $\{\mathbf{R}_s, \mathbf{w}_k\}$

By fixing $\boldsymbol{\theta}$, the subproblem with respect to $\{\mathbf{R}_s, \mathbf{w}_k\}$ can be expressed as

$$\begin{aligned} \mathcal{P}_2 : \quad & \max_{\mathbf{R}_s, \mathbf{w}_k} \sum_{k \in \mathcal{K}} R_k \\ \text{s.t.} \quad & \text{C1: } \text{tr} \left(\sum_{k \in \mathcal{K}} \mathbf{w}_k \mathbf{w}_k^H + \mathbf{R}_s \right) \leq P_t, \\ & \text{C2: } \max_{\substack{\Delta_{\text{aw}} \in \mathcal{U}_{\text{aw}} \\ \Delta_{\text{rw}} \in \mathcal{U}_{\text{rw}}}} D(\mathbb{P}_0 \| \mathbb{P}_1) \leq 2\varepsilon^2, \\ & \text{C3: } \text{tr}(\mathbf{C}) \leq \text{MSE}_{\text{max}}, \\ & \text{C5: } \mathbf{R}_s \succeq \mathbf{0}. \end{aligned} \quad (32)$$

However, problem \mathcal{P}_2 is still non-convex due to the non-convex constraints C2 and C3. To address this challenge, we first define $\mathbf{W}_k \triangleq \mathbf{w}_k \mathbf{w}_k^H$ that satisfies $\text{rank}(\mathbf{W}_k) = 1$ and $\mathbf{W}_k \succeq \mathbf{0}, \forall k$, then the objective function and constraints of \mathcal{P}_2 can be translated into more tractable forms as follows.

1) *Objective function of \mathcal{P}_2* : We can rewrite the objective function of \mathcal{P}_2 in the form of the difference of two concave functions, i.e.,

$$\begin{aligned} \sum_{k \in \mathcal{K}} R_k &= \sum_{k \in \mathcal{K}} \log_2 \left(\frac{\sum_{i \in \mathcal{K}} \mathbf{h}_k^H \mathbf{W}_i^H \mathbf{h}_k + \mathbf{h}_k^H \mathbf{R}_s \mathbf{h}_k + \sigma_{b,k}^2}{\sum_{i \in \mathcal{K}_k} \mathbf{h}_k^H \mathbf{W}_i^H \mathbf{h}_k + \mathbf{h}_k^H \mathbf{R}_s \mathbf{h}_k + \sigma_{b,k}^2} \right) \\ &= Q_1 - P_1, \end{aligned} \quad (33)$$

where

$$Q_1 \triangleq \sum_{k \in \mathcal{K}} \log_2 \left(\sum_{i \in \mathcal{K}} \mathbf{h}_k^H \mathbf{W}_i \mathbf{h}_k + \mathbf{h}_k^H \mathbf{R}_s \mathbf{h}_k + \sigma_{b,k}^2 \right), \quad (34)$$

$$P_1 \triangleq \sum_{k \in \mathcal{K}} \log_2 \left(\sum_{i \in \mathcal{K}_k} \mathbf{h}_k^H \mathbf{W}_i \mathbf{h}_k + \mathbf{h}_k^H \mathbf{R}_s \mathbf{h}_k + \sigma_{b,k}^2 \right).$$

Unfortunately, (33) is still a non-convex objective function. Thus, we adopt the SCA method to address this difficulty. For any feasible $\mathbf{W}^{(m)} = \{\mathbf{W}_k^{(m)}\}_{k \in \mathcal{K}}$ and $\mathbf{R}_s^{(m)}$, where m denotes the iteration index, P_1 could be upper bounded as

$$\begin{aligned} P_1 &\leq P_1^{(m)} + \text{tr} \left(\nabla_{\mathbf{R}_s}^H P_1^{(m)} \left(\mathbf{R}_s - \mathbf{R}_s^{(m)} \right) \right) \\ &\quad + \sum_{k \in \mathcal{K}} \text{tr} \left(\nabla_{\mathbf{w}_k}^H P_1^{(m)} \left(\mathbf{W}_k - \mathbf{W}_k^{(m)} \right) \right), \end{aligned} \quad (35)$$

where $P_1^{(m)} = P_1 \left(\mathbf{W}^{(m)}, \mathbf{R}_s^{(m)} \right)$ and

$$\begin{aligned} \nabla_{\mathbf{R}_s}^H P_1 \left(\mathbf{W}^{(m)}, \mathbf{R}_s^{(m)} \right) &= \\ \frac{1}{\ln 2} \sum_{j \in \mathcal{K}} \frac{\mathbf{h}_j \mathbf{h}_j^H}{\text{tr} \left(\mathbf{h}_j \mathbf{h}_j^H \mathbf{R}_s^{(m)} \right) + \sum_{i \in \mathcal{K}_j} \text{tr} \left(\mathbf{h}_j \mathbf{h}_j^H \mathbf{W}_i^{(m)} \right) + \sigma_{b,j}^2}, \\ \nabla_{\mathbf{w}_k}^H P_1 \left(\mathbf{W}^{(m)}, \mathbf{R}_s^{(m)} \right) &= \\ \frac{1}{\ln 2} \sum_{j \in \mathcal{K}_k} \frac{\mathbf{h}_j \mathbf{h}_j^H}{\text{tr} \left(\mathbf{h}_j \mathbf{h}_j^H \mathbf{R}_s^{(m)} \right) + \sum_{i \in \mathcal{K}_j} \text{tr} \left(\mathbf{h}_j \mathbf{h}_j^H \mathbf{W}_i^{(m)} \right) + \sigma_{b,j}^2}. \end{aligned}$$

Therefore, the original objective function in \mathcal{P}_2 can be transformed into a concave function based on the approximation in \mathcal{P}_2 to facilitate the design of an effective algorithm.

2) *Covertness constraint in C2*: We first introduce the following proposition to translate C2 into a tractable form.

Proposition 1 *Considering the channel estimation errors in (28), the covertness constraint in C2 can be equivalently transformed into*

$$\begin{aligned} \text{C2} &\Leftrightarrow \max_{\substack{\Delta_{\text{aw}} \in \mathcal{U}_{\text{aw}} \\ \Delta_{\text{rw}} \in \mathcal{U}_{\text{rw}}}} \left(\mathbf{h}_{\text{aw}}^H + \mathbf{h}_{\text{rw}}^H \boldsymbol{\Theta} \mathbf{G} \right) \mathbf{R} \left(\mathbf{h}_{\text{aw}}^H + \mathbf{h}_{\text{rw}}^H \boldsymbol{\Theta} \mathbf{G} \right)^H \\ &\leq (\eta_2 - 1) \sigma_w^2, \end{aligned} \quad (36)$$

where $\mathbf{R} = \mathbf{W}_c \mathbf{W}_c^H - (\eta_2 - 1) \mathbf{R}_s = \sum_{k \in \mathcal{K}} \mathbf{W}_k - (\eta_2 - 1) \mathbf{R}_s$, and $\eta_2 \geq 1$ is the solution to the equation $\ln x + \frac{1}{x} - 1 - \frac{2\varepsilon^2}{L} = 0$.

Proof: Let $h(x) = \ln x + \frac{1}{x} - 1 - \frac{2\varepsilon^2}{L}$. Then, it can be readily seen that there exist two roots η_1 and η_2 (assuming that $\eta_1 < 1 < \eta_2$) that satisfy $h(x) = 0$. Consequently, C2 can be equivalently converted to

$$\max_{\substack{\Delta_{\text{aw}} \in \mathcal{U}_{\text{aw}} \\ \Delta_{\text{rw}} \in \mathcal{U}_{\text{rw}}}} D(\mathbb{P}_0 \| \mathbb{P}_1) \leq 2\varepsilon^2 \stackrel{(a)}{\Leftrightarrow} \max_{\substack{\Delta_{\text{aw}} \in \mathcal{U}_{\text{aw}} \\ \Delta_{\text{rw}} \in \mathcal{U}_{\text{rw}}}} \frac{\lambda_1}{\lambda_0} \leq \eta_2, \quad (37)$$

where (a) holds because $\frac{\lambda_1}{\lambda_0} \geq 1$ and the fact that $h(x)$ is monotonically increasing when $x \geq 1$. Furthermore, based on the expression of \mathbf{h}_w^H defined in (22), we have

$$\begin{aligned} \max_{\substack{\Delta_{\text{aw}} \in \mathcal{U}_{\text{aw}} \\ \Delta_{\text{rw}} \in \mathcal{U}_{\text{rw}}}} \frac{\lambda_1}{\lambda_0} \leq \eta_2 &\Leftrightarrow \max_{\substack{\Delta_{\text{aw}} \in \mathcal{U}_{\text{aw}} \\ \Delta_{\text{rw}} \in \mathcal{U}_{\text{rw}}}} \frac{\mathbf{h}_w^H \mathbf{W}_c \mathbf{W}_c^H \mathbf{h}_w}{\mathbf{h}_w^H \mathbf{R}_s \mathbf{h}_w + \sigma_w^2} \leq \eta_2 - 1 \\ &\Leftrightarrow \max_{\substack{\Delta_{\text{aw}} \in \mathcal{U}_{\text{aw}} \\ \Delta_{\text{rw}} \in \mathcal{U}_{\text{rw}}}} \left(\mathbf{h}_{\text{aw}}^H + \mathbf{h}_{\text{rw}}^H \boldsymbol{\Theta} \mathbf{G} \right) \mathbf{R} \left(\mathbf{h}_{\text{aw}}^H + \mathbf{h}_{\text{rw}}^H \boldsymbol{\Theta} \mathbf{G} \right)^H \\ &\leq (\eta_2 - 1) \sigma_w^2. \end{aligned} \quad (38)$$

The proof is thus completed. \blacksquare

Although the transformed form in (36) is more tractable than the original form in C2, it is still non-convex due to the continuity of the CSI uncertainty sets \mathcal{U}_{aw} and \mathcal{U}_{rw} . To tackle this issue, we introduce the following Lemma and transform the non-convex constraint in (36) into a more tractable form in terms of linear matrix inequality (LMI).

Lemma 1 (*S-Procedure [32]*): *Let*

$$f_i(\mathbf{x}) = \mathbf{x}^H \mathbf{P}_i \mathbf{x} + 2\Re \{ \mathbf{q}_i^H \mathbf{x} \} + q_i, \quad i \in [0, P], \quad (39)$$

where $\mathbf{P}_i \in \mathbb{H}^N, \mathbf{q}_i \in \mathbb{C}^N$ and $q_i \in \mathbb{R}$. Then, the implication relation $f_0(\mathbf{x}) \leq 0$ for all \mathbf{x} with $\{f_i(\mathbf{x}) \leq 0\}_{i=1}^P$ holds if and only if there exists a variable $\mu_i \geq 0$ such that

$$\sum_{i=1}^P \mu_i \begin{bmatrix} \mathbf{P}_i & \mathbf{q}_i \\ \mathbf{q}_i^H & q_i \end{bmatrix} \succeq \begin{bmatrix} \mathbf{P}_0 & \mathbf{q}_0 \\ \mathbf{q}_0^H & q_0 \end{bmatrix}. \quad (40)$$

Based on Lemma 1, the following Proposition 2 that can transform (36) into an LMI form is presented.

Proposition 2 *By inserting (28) into the covertness constraint in (36), C2 can be equivalently transformed into the following form⁴*

$$\text{C2} \Leftrightarrow \overline{\text{C2a}} : \boldsymbol{\Pi} \triangleq \begin{bmatrix} \mathbf{P} + \boldsymbol{\mu} & \mathbf{q} \\ \mathbf{q}^H & q \end{bmatrix} \succeq \mathbf{0} \text{ and } \overline{\text{C2b}} : \mu_1, \mu_2 \geq 0, \quad (41)$$

⁴Different from [21], the LMI form obtained based on Proposition 2 is more concise. Moreover, the dimension of the LMI in (41) is $N_A + N_R + 1$, which entails much lower computational complexity as compared to the LMI with dimension $N_A + N_A N_R + 1$ in [21].

where \mathbf{P} , $\boldsymbol{\mu}$, and q are given in Appendix A, $\mu_1 \geq 0$ and $\mu_2 \geq 0$ are slack variables.

Proof: Please refer to Appendix A. \blacksquare

3) *Sensing MSE constraint in C3:* To deal with the non-convex constraint C3, we first introduce auxiliary variables $c_i \geq 0$, $i \in \{1, \dots, 6\}$ to bound the diagonal entries of the posterior covariance matrix \mathbf{C} , i.e., $\{\mathbf{C}\}_{ii} \leq c_i$. Then, C3 in (32) can be equivalently rewritten as

$$\overline{\text{C3a}} : \sum_{i=1}^6 m_i \leq \text{MSE}_{\max} \text{ and } \overline{\text{C3b}} : \begin{bmatrix} \mathbf{C}^{-1} & \mathbf{e}_i \\ \mathbf{e}_i^T & c_i \end{bmatrix} \succeq \mathbf{0}, \forall i, \quad (42)$$

where $\mathbf{e}_i \in \mathbb{R}^{6 \times 1}$ is the i -th column of \mathbf{I}_6 .

Based on the derivation above, problem $\mathcal{P}2$ can be rewritten as

$$\begin{aligned} \bar{\mathcal{P}}_2 : \quad & \max_{\mathbf{R}_s, \mathbf{W}_k, \lambda_1, \lambda_2, c_i} Q_1 - \bar{P}_1 \\ \text{s.t.} \quad & \text{C1} : \text{tr} \left(\sum_{k \in \mathcal{K}} \mathbf{W}_k + \mathbf{R}_s \right) \leq P_t, \\ & \overline{\text{C2a}} - \overline{\text{C2b}} : (41), \quad \overline{\text{C3a}} - \overline{\text{C3b}} : (42), \\ & \text{C5} : \mathbf{R}_s \succeq \mathbf{0}, \quad \text{C6} : \mathbf{W}_k \succeq \mathbf{0}, \forall k, \\ & \text{C7} : \text{rank}(\mathbf{W}_k) = 1, \forall k, \end{aligned} \quad (43)$$

where $\bar{P}_1 = \sum_{k \in \mathcal{K}} \text{tr}(\nabla_{\mathbf{W}_k}^H P_1(\mathbf{W}^{(m)}, \mathbf{R}_s^{(m)}) \mathbf{W}_k) + \text{tr}(\nabla_{\mathbf{R}_s}^H P_1(\mathbf{W}^{(m)}, \mathbf{R}_s^{(m)}) \mathbf{R}_s)$.

Omitting the rank-one constraint C7, $\bar{\mathcal{P}}_2$ is jointly convex with respect to \mathbf{R}_s , \mathbf{W}_k , λ_1 , λ_2 , and c_i , which can be solved by off-the-shelf convex optimization solvers, such as CVX [33]. In fact, if the relaxed problem is feasible, the rank-one constraints C7 can always be satisfied, as we will prove in Proposition 3.

Proposition 3 *If the relaxed problem $\bar{\mathcal{P}}_2$ is feasible, the optimal solution \mathbf{W}_k^* always satisfies the rank-one condition C7.*

Proof: Please refer to Appendix B. \blacksquare

D. Subproblem With Respect to $\{\boldsymbol{\theta}\}$

Then, fixing $\{\mathbf{R}_s, \mathbf{w}_k\}$, the RIS phase-shift design subproblem is given by

$$\begin{aligned} \mathcal{P}_3 : \quad & \max_{\boldsymbol{\theta}} \sum_{k \in \mathcal{K}} R_k \\ \text{s.t.} \quad & \text{C2} : \max_{\substack{\Delta_{\text{aw}} \in \mathcal{U}_{\text{aw}} \\ \Delta_{\text{rw}} \in \mathcal{U}_{\text{rw}}}} D(\mathbb{P}_0 \| \mathbb{P}_1) \leq 2\varepsilon^2, \\ & \text{C4} : |\theta_i|^2 = 1, \quad i \in [1 : N_R], \end{aligned} \quad (44)$$

where the remaining non-convexity is caused by C2 and C4. Similar to Section III-C, we will transform the constraints and objective function in \mathcal{P}_3 into tractable forms. Before handling this challenging issue, we first introduce an auxiliary variable $\beta \in \mathbb{C}$ with $|\beta| = 1$ and then define

$$\mathbf{v} \triangleq [\beta \boldsymbol{\theta}^H, \beta]^T, \quad \mathbf{V} \triangleq \mathbf{v} \mathbf{v}^H = \begin{bmatrix} \boldsymbol{\theta}^* \boldsymbol{\theta}^T & \boldsymbol{\theta}^* \\ \boldsymbol{\theta}^T & 1 \end{bmatrix}. \quad (45)$$

1) *Objective function of \mathcal{P}_3 :* We first define $\mathbf{G}_k \triangleq \text{diag}(\mathbf{h}_{r,k}^H) \mathbf{G}$, $\mathbf{T}_k \triangleq [\mathbf{G}_k^H, \mathbf{h}_{d,k}]$, $\Phi_{k,i} \triangleq \mathbf{T}_k^H \mathbf{W}_i \mathbf{T}_k$ and $\Psi_k \triangleq \mathbf{T}_k^H \mathbf{R}_s \mathbf{T}_k$. Then, based on (34), we can rewrite Q_1 as follows

$$\begin{aligned} Q_1 &= \sum_{k \in \mathcal{K}} \log_2 \left(\sum_{i \in \mathcal{K}} \mathbf{h}_k^H \mathbf{W}_i \mathbf{h}_k + \mathbf{h}_k^H \mathbf{R}_s \mathbf{h}_k + \sigma_{b,k}^2 \right) \\ &= \sum_{k \in \mathcal{K}} \log_2 \left(\begin{aligned} & \text{tr}(\boldsymbol{\theta}^* \boldsymbol{\theta}^T \mathbf{G}_k (\sum_{i \in \mathcal{K}} \mathbf{W}_i + \mathbf{R}_s) \mathbf{G}_k^H) \\ & + \boldsymbol{\theta}^* \mathbf{h}_{d,k}^H (\sum_{i \in \mathcal{K}} \mathbf{W}_i + \mathbf{R}_s) \mathbf{G}_k^H \\ & + \boldsymbol{\theta}^T \mathbf{G}_k (\sum_{i \in \mathcal{K}} \mathbf{W}_i + \mathbf{R}_s) \mathbf{h}_{d,k} \\ & + \mathbf{h}_{d,k}^H (\sum_{i \in \mathcal{K}} \mathbf{W}_i + \mathbf{R}_s) \mathbf{h}_{d,k} + \sigma_{b,k}^2 \end{aligned} \right) \\ &= \sum_{k \in \mathcal{K}} \log_2 \left(\sum_{i \in \mathcal{K}} \text{tr}(\Phi_{k,i} \mathbf{V}) + \text{tr}(\Psi_k \mathbf{V}) + \sigma_{b,k}^2 \right). \end{aligned} \quad (46)$$

Similarly, P_1 can be equivalently transformed into

$$P_1 = \sum_{k \in \mathcal{K}} \log_2 \left(\sum_{j \in \mathcal{K}_k} \text{tr}(\Phi_{k,j} \mathbf{V}) + \text{tr}(\Psi_k \mathbf{V}) + \sigma_{b,k}^2 \right). \quad (47)$$

To tackle the non-concavity of the objective function, we adopt a similar SCA method as in (35) to handle P_1 . Specifically, for any feasible $\mathbf{V}^{(m)}$, P_1 can be upper bounded as

$$P_1 \leq P_1^{(m)} + \text{tr} \left(\nabla_{\mathbf{V}}^H P_1(\mathbf{V}^{(m)}) (\mathbf{V} - \mathbf{V}^{(m)}) \right), \quad (48)$$

where

$$\begin{aligned} & \nabla_{\mathbf{V}}^H P_1(\mathbf{V}^{(m)}) \\ &= \frac{1}{\ln 2} \sum_{k \in \mathcal{K}} \frac{\sum_{j \in \mathcal{K}_k} \Phi_{k,j} + \Psi_k}{\sum_{j \in \mathcal{K}_k} \text{tr}(\Phi_{k,j} \mathbf{V}^{(m)}) + \text{tr}(\Psi_k \mathbf{V}^{(m)}) + \sigma_{b,k}^2}. \end{aligned}$$

2) *Covertness constraint in C2:* By leveraging the following proposition, the infinite infinitely many constraints of C2 in (44) can be transformed into an LMI form with respect to \mathbf{V} .

Proposition 4 *By inserting (28) into the covertness constraint in (44), C2 can be equivalently transformed into the following form*

$$\text{C2} \Leftrightarrow \overline{\text{C2a}} : \overline{\boldsymbol{\Pi}} \triangleq \begin{bmatrix} \hat{\mathbf{P}} + \hat{\boldsymbol{\mu}} & \hat{\mathbf{q}} \\ \hat{\mathbf{q}}^H & \hat{q} \end{bmatrix} \succeq \mathbf{0} \text{ and } \overline{\text{C2b}} : \hat{\mu}_1, \hat{\mu}_2 \geq 0, \quad (49)$$

where $\hat{\mathbf{P}}$, $\hat{\boldsymbol{\mu}}$, and \hat{q} are given in Appendix C, $\hat{\mu}_1 \geq 0$ and $\hat{\mu}_2 \geq 0$ are slack variables.

Proof: Please refer to Appendix C. \blacksquare

3) *The non-convex unit-modulus constraints in C4:* Based on the definition in (45), the non-convex unit-modulus constraints in C4 can be equivalently represented as

$$\begin{aligned} \text{C4} \Leftrightarrow \text{C8} : \text{diag}(\mathbf{V}) &= \mathbf{1}_{N_R+1}, \\ \text{C9} : \mathbf{V} &\succeq \mathbf{0} \text{ and } \text{C10} : \text{rank}(\mathbf{V}) = 1, \end{aligned} \quad (50)$$

where C8 can guarantee the unit modulus of $\boldsymbol{\theta}$, C9 and C10 are introduced to guarantee that $\mathbf{V} = \mathbf{v} \mathbf{v}^H$.

The non-convexity of constraint C10 is addressed by adopting the sequential rank-one constraint relaxation (SROCR) technique, which systematically relaxes the rank-one condition via a progressive relaxation strategy. Unlike conventional rank-one relaxation approaches [34] that completely discard this constraint, the SROCR method achieves computationally tractable solutions while preserving essential problem structure through controlled constraint relaxation. In particular, we first

equivalently rewrite the rank-one constraint as [35]

$$\text{C10} \Leftrightarrow \overline{\text{C10}} : \lambda_{\max}(\mathbf{V}) = \text{tr}(\mathbf{V}) = \max_{\substack{\mathbf{x} \in \mathbb{C}^{(N_{\text{R}}+1) \times 1}, \\ \|\mathbf{x}\|_2 \leq 1}} \mathbf{x}^H \mathbf{V} \mathbf{x}, \quad (51)$$

where \mathbf{x} is a slack vector and the second equality holds if and only if $\mathbf{x} = \mathbf{u}_{\max}(\mathbf{V})$.

According to [34], the basic idea of SROCR is to partially relax the rank one constraint $\overline{\text{C10}}$ in (51) as

$$\overline{\overline{\text{C10}}} : \mathbf{u}_{\max}^H(\mathbf{V}^{(m)}) \mathbf{V} \mathbf{u}_{\max}(\mathbf{V}^{(m)}) \geq \widehat{\mu}_3^{(m)} \text{tr}(\mathbf{V}^{(m)}), \quad (52)$$

where $\widehat{\mu}_3^{(m)}$ is a slack parameter to control the ratio of the largest eigenvalue of \mathbf{V} to the trace of \mathbf{V} , and the rank-one constraint is satisfied until $\widehat{\mu}_3^{(m)}$ increases to 1.

Based on the above derivations, the final optimization problem of θ can be rewritten as

$$\begin{aligned} \overline{\mathcal{P}}_3 : & \max_{\mathbf{V}, \mu_1, \mu_2} Q_1 - \overline{P}_1 \\ \text{s.t.} & \overline{\text{C2a}} - \overline{\text{C2b}} : (49), \text{C8} : \text{diag}(\mathbf{V}) = \mathbf{1}_{N_{\text{R}}+1}, \\ & \text{C9} : \mathbf{V} \succeq \mathbf{0}, \overline{\overline{\text{C10}}} : (52). \end{aligned} \quad (53)$$

where $\overline{P}_1 = \text{tr}(\nabla_{\mathbf{V}}^H P_2(\mathbf{V}^{(m)}) \mathbf{V})$. It is readily observed that $\overline{\mathcal{P}}_3$ is convex and can be solved by existing convex optimization solvers. In particular, the slack parameter $\widehat{\mu}_3^{(m+1)}$ can be updated by

$$\widehat{\mu}_3^{(m+1)} = \min(1, \frac{\lambda_{\max}(\mathbf{V}^{(m)})}{\text{tr}(\mathbf{V}^{(m)})} + \delta^{(m)}), \quad (54)$$

where $\delta^{(m)}$ is the step size that is reduced iteratively by $\delta^{(m+1)} = \frac{\delta^{(m)}}{2}$ until $\overline{\mathcal{P}}_3$ is solvable [34].

Algorithm 1 AO-based algorithm to solve problem \mathcal{P}_1

Input: $\varepsilon, \text{MSE}_{\max}, P_t$.

- 1: Set the outer iteration index $m_o = 0$ and initialize $\mathbf{W}_k^{(0)}, \mathbf{R}_s^{(0)}, \theta^{(0,0)}$.
 - 2: **repeat**
 - 3: Update $\{\mathbf{R}_s^{(m_o+1)}, \mathbf{W}_k^{(m_o+1)}\}$ by solving $\overline{\mathcal{P}}_2$ with given $\{\mathbf{R}_s^{(m_o)}, \mathbf{W}_k^{(m_o)}\}$.
 - 4: Set $\mathbf{V}^{(m_o,0)}$ with given $\theta^{(m_o,0)}$ according to (45).
 - 5: Initialize the step size $\delta^{(0)}$, set the inner iteration index $m_i = 0$ and the slack parameter $\widehat{\mu}_3^{(0)} = 0$.
 - 6: **repeat**
 - 7: **if** $\overline{\mathcal{P}}_3$ is feasible **then**
 - 8: Update $\mathbf{V}^{(m_o, m_i+1)}$ by solving $\overline{\mathcal{P}}_3$ in (53) with given $\mathbf{V}^{(m_o, m_i)}$.
 - 9: Update $\delta^{(m_i+1)} = \delta^{(m_i)}$.
 - 10: **else**
 - 11: Update $\delta^{(m_i+1)} = \frac{\delta^{(m_i)}}{2}$.
 - 12: **end if**
 - 13: Update $\widehat{\mu}_3^{(m_i+1)}$ according to (54).
 - 14: $m_i = m_i + 1$.
 - 15: **until** $(f_{\overline{\mathcal{P}}_3}^{(m_o, m_i+1)} - f_{\overline{\mathcal{P}}_3}^{(m_o, m_i)}) / f_{\overline{\mathcal{P}}_3}^{(m_o, m_i)} \leq \varepsilon_{\text{in},1}$ and $\lambda_{\max}(\mathbf{V}^{(m_o, m_i+1)}) / \text{tr}(\mathbf{V}^{(m_o, m_i+1)}) \leq \varepsilon_{\text{in},2}$.
 - 16: Obtain $\theta^{(m_o+1,0)}$ by decomposing $\mathbf{V}^{(m_o, m_i)}$ and $m_o = m_o + 1$.
 - 17: **until** $\sum_{k \in \mathcal{K}} (R_k^{(m_o+1)} - R_k^{(m_o)}) / \sum_{k \in \mathcal{K}} R_k^{(m_o)} \leq \varepsilon_{\text{out}}$.
- Output:** $\{\mathbf{W}_k, \mathbf{R}_s, \theta\}$.
-

Finally, Algorithm 1 summarizes all the key steps of solving the original problem in \mathcal{P}_1 , where $f_{\overline{\mathcal{P}}_3}$ denotes the objective

function value in $\overline{\mathcal{P}}_3$. After optimizing the communication beamformers, the covariance matrix of the sensing signal, and the RIS phase shifts, Alice (assisted by RIS) can transmit communication signals covertly and meanwhile send the sensing signal to sense Willie. At the same time, based on the echo signal of the sensing signal, Alice will obtain the new measurements about Willie in time slot n and then correct the estimated state information of Willie as mentioned in Section III-A.

E. Convergence and Complexity analysis

It is worth noting that we can obtain a lower bound on the optimal objective value of \mathcal{P}_2 by solving $\overline{\mathcal{P}}_2$. Then, According to [34, Theorem 1], the SROCR-based method can converge to a KKT solution of $\overline{\mathcal{P}}_3$ with the original rank-one constraint C10, which means that the lower bound of the optimal objective values of \mathcal{P}_3 can still be obtained by solving $\overline{\mathcal{P}}_3$. Finally, we can monotonically tighten these lower bounds by alternatively optimizing $\{\mathbf{W}_k, \mathbf{R}_s\}$ and $\{\theta\}$. The objective values achieved by the sequence $\{\mathbf{W}_k^{(m_o)}, \mathbf{R}_s^{(m_o)}, \theta^{(m_o,0)}\}_{m_o \in \mathbb{N}}$ form a non-decreasing sequence that converges to a stationary value in polynomial time, and any limit point of the sequence $\{\mathbf{W}_k^{(m_o)}, \mathbf{R}_s^{(m_o)}, \theta^{(m_o,0)}\}_{m_o \in \mathbb{N}}$ is a stationary point of the original problem \mathcal{P}_1 [36].

Moreover, it is clear that the main complexity of Algorithm 1 arises from solving $\overline{\mathcal{P}}_2$ and $\overline{\mathcal{P}}_3$, and the approximated complexity of utilizing the interior point method to solve them are $\mathcal{O}((K+3)N_{\text{A}}^{3.5} + (K+3)^2 N_{\text{A}}^{2.5} + K^3)$ and $\mathcal{O}(l_2(3N_{\text{R}}^{3.5} + 18N_{\text{R}}^{2.5} + 27N_{\text{R}}^{1.5}))$, respectively, where l_2 denotes the iteration number required for solving $\overline{\mathcal{P}}_3$. Therefore, the total complexity of Algorithm 1 is given by $\mathcal{O}(l_{\text{AO}}((K+3)N_{\text{A}}^{3.5} + (K+3)^2 N_{\text{A}}^{2.5} + K^3) + \mathcal{O}(l_{\text{AO}} l_2(3N_{\text{R}}^{3.5} + 18N_{\text{R}}^{2.5} + 27N_{\text{R}}^{1.5}))$, where l_{AO} is the number of outer iterations.

IV. SIMULATION RESULTS

In this section, we present some simulation results to evaluate the effectiveness of the proposed algorithms. We consider a RIS-empowered ISCC system as shown in Fig. 3, where Alice and RIS are located at $[0 \text{ m}, 0 \text{ m}, 10 \text{ m}]$ and $[60 \text{ m}, 60 \text{ m}, 10 \text{ m}]$, respectively. The legitimate communication users, i.e., Bobs, are randomly and uniformly distributed within a radius of 5 m in a circle centered at $[45 \text{ m}, 90 \text{ m}, 10 \text{ m}]$, the number of Bobs is set as $K = 4$, and each Alice-Bob k link follows the Rayleigh flat fading model [37]. The large-scale fading of all channels are modeled as $PL = \rho_0 - 10\alpha \log_{10}(d)$ dB with the path loss exponent α and the link distance d in meter [37]. We consider a mobile Willie (such as UAV) with its flight speed fixed at 20 m/s, and the variation of Willie direction is randomly distributed in $[-\pi/18, 0]$. The convergence threshold related parameters of Algorithm 1 are set as $\varepsilon_{\text{out}} = \varepsilon_{\text{in},1} = 10^{-4}$ and $\varepsilon_{\text{in},2} = 0.999$. Other specific system parameters adopted for our simulations are listed in Table I.

To verify the efficiency of the proposed algorithm, we also compare it with two baseline schemes as follows:

- **Baseline 1:** In this case, we extend the single user scenario in [18] to a multi-user scenario, while assuming that RIS is not deployed. Similar to [38], we optimize the communication beamformers and sensing signal covariance matrix by setting $\Theta = \mathbf{I}_{N_{\text{R}}}$ and then solve $\overline{\mathcal{P}}_2$ in (43).

TABLE I: System Parameters

Parameter	Value	Parameter	Value
Number of Antenna at Alice	$[N_H, N_V] = [5, 2]$	Frame duration	$T = 7$ s
Number of Passive elements at RIS	$N_R = 8 \sim 16$	Slot duration	$\delta = 0.1$ s
RCS of Willie	$\zeta = 1$	Number of symbols in each slot	$L = 1000$
Noise power at Bob	$\sigma_{b,1}^2 = \dots = \sigma_{b,K}^2 = -90$ dBm	Matched-filter gain	$G_{MF} = 1000$
Noise power at Willie	$\sigma_w^2 = -90$ dBm	Center frequency	$f_c = 3$ GHz
Noise power at Alice for sensing	$\sigma_r^2 = -100$ dBm	Modeling parameter of τ_w	$c_{\tau_w} = 10^{-6}$
Transmit power at Alice	$P_t = 26 \sim 34$ dBm	Modeling parameter of v_w	$c_{v_w} = 10^5$
Covertness level	$\varepsilon = 0.05 \sim 0.25$	Modeling parameter of θ_{aw}	$c_{\theta_{aw}} = 1$
Sensing threshold	$MSE_{max} = 7 \sim 12$	Modeling parameter of ϕ_{aw}	$c_{\phi_{aw}} = 1$
Path loss exponents of RIS-Bob link	$\alpha_{RB,1} = \dots = \alpha_{RB,K} = 2$	Channel power at one meter	$\rho_0 = -30$ dB
Path loss exponents of Alice-Bob link	$\alpha_{AB,1} = \dots = \alpha_{AB,K} = 4$	Path loss exponents of Alice-RIS link	$\alpha_{AR} = 2.2$

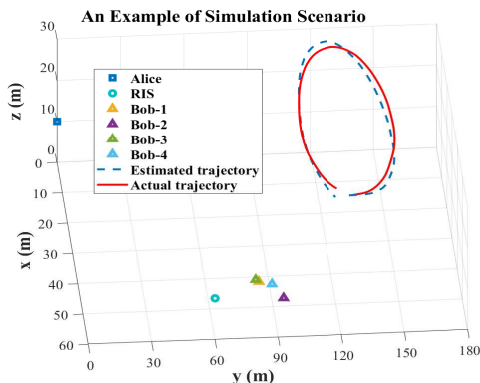
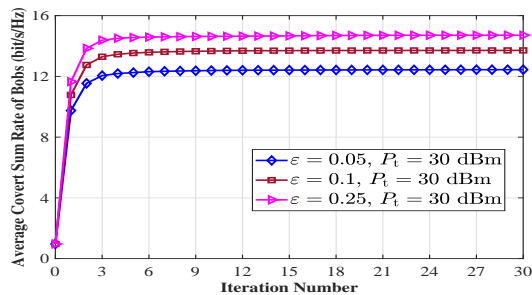


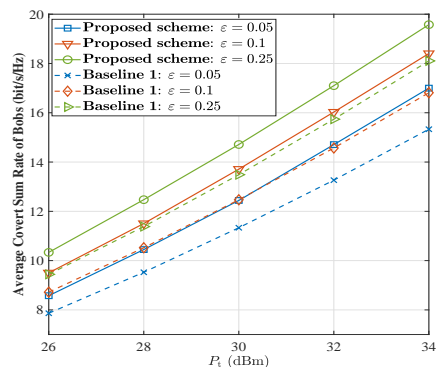
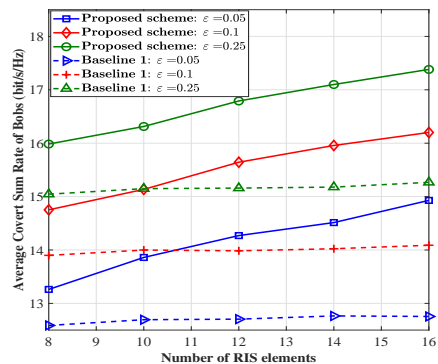
Fig. 3: An example of our simulation scenario.

Fig. 4: Convergence properties of Algorithm 1 with $N_A = N_R = 10$ and $MSE_{max} = 7$.

- **Baseline 2:** In this case, we consider a non-robust design scheme that ignores the channel estimation errors in (6), i.e., the covert design in (26) directly using $\hat{\mathbf{h}}_{aw}$ and $\hat{\mathbf{h}}_{rw}$ instead of \mathbf{h}_{aw} and \mathbf{h}_{rw} [5], [9].

We first investigate the convergence properties of the proposed Algorithm 1 with $N_A = N_R = 10$ and $MSE_{max} = 7$. Fig. 4 shows the relationship between the average covert sum rate of Bobs and the iteration number of the algorithm with different covertness levels and transmit powers at Alice. It can be observed that the proposed Algorithm 1 quickly converges to a steady value after about 6 iterations. Meanwhile, setting a more relaxed covertness level constraint can also improve the covert sum rate. This is because the more relaxed covertness level constraint prevents Alice from excessively reducing the energy of communication beamformers to meet the covert requirements and achieves a better covert sum rate.

Then, for the same setting above and for a fixed time slot, Fig. 5 illustrates the average covert sum rate of Bobs versus the maximum transmit power P_t at Alice. It can be seen that the covert sum rate of Bobs increases monotonically with the increasing of the maximum transmit power at Alice. In addition, Fig. 5 also shows that the average covert sum rate

Fig. 5: Average covert sum rate of Bobs versus the maximum transmit power with $N_A = N_R = 10$ and $MSE_{max} = 7$.Fig. 6: Average covert sum rate of Bobs versus the number of RIS elements with $N_A = 10$, $P_t = 30$ dBm and $MSE_{max} = 7$.

of our proposed algorithm exceeds that of Baseline 1, since optimizing the passive elements of RIS can reconfigure the channel environment to facilitate improving the covert sum rate of Bobs as compared to not deploying RIS.

Fig. 6 further compares the average covert sum rate of Bobs versus the numbers of passive elements at RIS at the IRS. By increasing the number of passive elements at RIS, the RIS-empowered ISCC system demonstrates a more significant improvement in the average covert sum rate compared to Baseline 1 with the same covertness level. This is due to the fact that additional passive elements can reflect more of the power received from Alice to improve the beamforming gain and then achieve a better average covert sum rate. Meanwhile, Fig. 6 also reveals that enlarging the RIS size can be conducive to achieving a stricter covertness level at the same average covert sum rate of Bobs, which provides another degree of freedom to satisfy covert communication constraints rather than simply controlling the power allocation between communication and sensing.

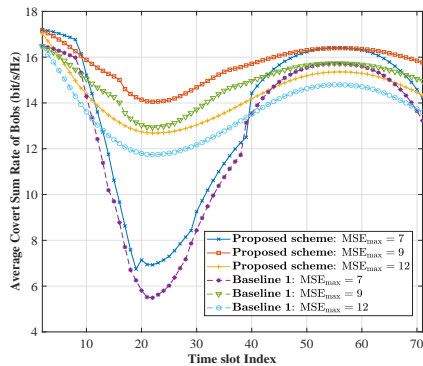


Fig. 7: Average covert sum rate of Bobs versus the time slot index with $N_A = N_R = 10$ and $\varepsilon = 0.25$.

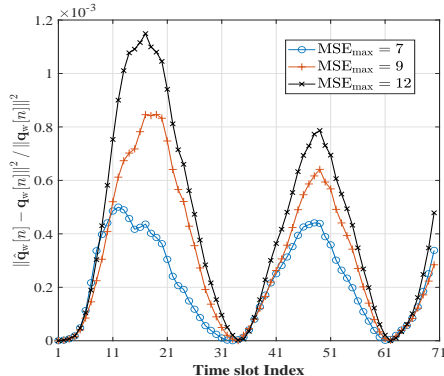


Fig. 8: The corresponding normalized posterior MSE of tracking Willie's location versus the time slot index with $N_A = N_R = 10$ and $\varepsilon = 0.25$.

Next, we examine the tracking performance and the effective covert sum rate variation in a tracking period with $N_A = N_R = 10$. Specifically, Fig. 7 illustrates the average covert sum rate of Bobs versus time slot index throughout the entire process of tracking Willie. It can be seen that the performance of our proposed scheme is always superior to that of Baseline 1 throughout the entire process simulated. However, the covert sum rate is not constant and drops in some time slots. This is because the posterior MSE for tracking the adversary target is accumulated over the time, causing Alice to allocate more power to sensing in order to meet the sensing constraints and this situation will be improved as the EKF-based method can track Willie well to reduce the posterior MSE. This tracking MSE variation is further illustrated in Fig. 8, where the corresponding normalized posterior MSE of tracking Willie's location, i.e., $\|\hat{\mathbf{q}}_w[n] - \mathbf{q}_w[n]\|^2 / \|\mathbf{q}_w[n]\|^2$, is evaluated for each time slot. Moreover, a comparison of the covert sum rate under different MSE_{\max} constraints reveals that stricter sensing constraint (e.g., $MSE_{\max} = 7$) leads to a more significant reduction in the covert rate in the tracking process. This occurs because a greater portion of the available power is allocated to sensing for ensuring tracking accuracy.

We also demonstrate the robustness of the proposed scheme in terms of covertness through simulation. In particular, Fig. 9 illustrates the empirical cumulative density function (CDF) of the achieved $D(\mathbb{P}_0||\mathbb{P}_1)$ under the covertness thresholds $\varepsilon = 0.05$ and $\varepsilon = 0.01$, respectively, where we fix $N_A = N_R = 10$, $MSE_{\max} = 7$ and $P_t = 30$ dBm. It is evident that the proposed scheme demonstrates superior robustness concerning covertness requirements compared to Baseline 2 (non-robust design). Specifically, approximately 20% of the resulting $D(\mathbb{P}_0||\mathbb{P}_1)$ does not exceed $2\varepsilon^2 = 0.005$, and

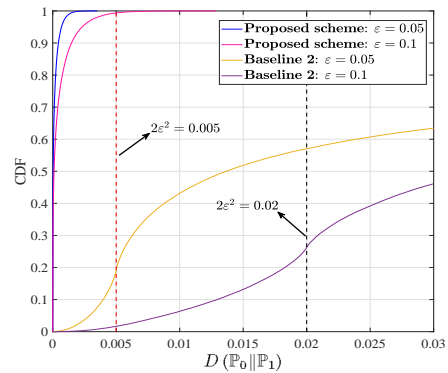


Fig. 9: The empirical CDF of the achieved $D(\mathbb{P}_0||\mathbb{P}_1)$ with $N_A = N_R = 10$, $MSE_{\max} = 7$ and $P_t = 30$ dBm.

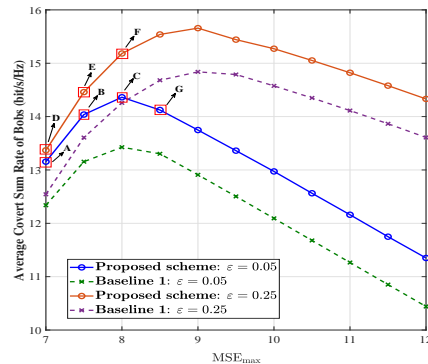


Fig. 10: Tradeoff between the covert sum rate and sensing MSE_{\max} with $N_A = N_R = 10$ and $P_t = 30$ dBm.

about 26.3% does not exceed $2\varepsilon^2 = 0.02$ in Baseline 2. In contrast, our proposed scheme consistently satisfies the covertness requirement, underscoring the effective robustness of our scheme.

Finally, we analyze the tradeoff between covert communication and sensing performance by evaluating the covert sum rate averaged over multiple time slots in a tracking period as a function of the sensing constraint MSE_{\max} . As shown in Fig. 10, the average covert sum rate initially increases and then decreases as the sensing requirement MSE_{\max} is gradually relaxed. Specifically, a smaller MSE_{\max} demands more power to be allocated to sensing, which improves tracking accuracy and channel estimation for Willie. However, this reduces the power available for communication, leading to a lower effective covert sum rate. Conversely, as MSE_{\max} increases, relaxing the sensing constraint (C3) allows more power for communication, resulting in a higher covert sum rate (e.g., from Point A to Point C with $\varepsilon = 0.05$). Beyond a certain point, however, further relaxation of MSE_{\max} introduces greater uncertainty in the predicted CSI of Willie, which degrades covert efficiency and causes the covert sum rate to decrease (e.g., from Point C to Point G with $\varepsilon = 0.05$). It is also noted that the exact tradeoff curve depends on the level of covertness.

Fig. 11 further presents the power allocation outcomes for different covertness levels, which align with the earlier discussions. It can be seen that under a stricter covert requirement (e.g., $\varepsilon = 0.05$), improving the tracking MSE from Point C to Point A requires only an additional 3.6289% of power allocated to sensing. In contrast, under a more relaxed covertness requirement ($\varepsilon = 0.25$), this additional power allocated to sensing increases to 11.4503% from Point F to Point D. These differences arise because, under stricter covert

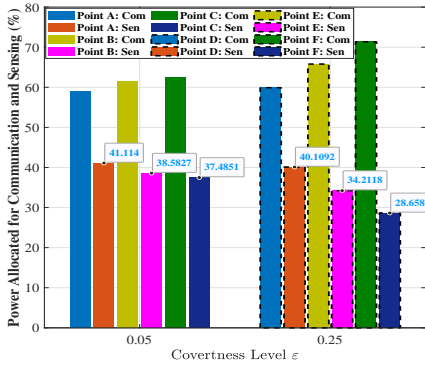


Fig. 11: The average power allocation strategy between the sensing and communication with $N_A = N_R = 10$ and $P_t = 30$ dBm.

requirements, Alice tends to allocate more power to sensing to reduce the KL divergence and meet the covertess constraint. As a result, less additional power is needed to achieve further improvements in tracking.

V. CONCLUSION

This paper has proposed a sensing-then-beamforming framework for RIS-empowered ISCC systems. This framework leverages sensing capabilities to track and predict the state of a mobile warden Willie and construct the corresponding channels. Accounting for the constructed channel errors, we have formulated a robust non-convex optimization problem for the joint design of the beamformers and sensing signal covariance matrix at Alice, as well as the phase shifts at the RIS, aiming to maximize the covert sum rate of multiple legitimate Bobs. The structural properties of the problem have been analyzed and exploited to transform it into a more tractable form. An alternating-optimization-based algorithm has been developed to iteratively solve subproblems concerning Alice and RIS separately. Simulation results verified the effectiveness of our proposed scheme and demonstrated its superior performance compared to baseline designs.

Future work could extend the current framework to address scenarios involving multiple wardens. Additionally, the framework could be explored for sensing-assisted covert communication in environments with more complex scattering characteristics. Moreover, it would be intriguing to explore a fully integrated dual-functional waveform that simultaneously protects both communication and sensing functions for the ISCC system.

APPENDIX A PROOF OF PROPOSITION 2

By substituting (28) into the left term of (36), we have

$$\begin{aligned}
& (\mathbf{h}_{\text{aw}}^H + \mathbf{h}_{\text{rw}}^H \Theta \mathbf{G}) \mathbf{R} (\mathbf{h}_{\text{aw}}^H + \mathbf{h}_{\text{rw}}^H \Theta \mathbf{G})^H \\
&= (\Delta_{\text{rw}}^H \Theta \mathbf{G} + \Delta_{\text{aw}}^H) \mathbf{R} (\Delta_{\text{rw}}^H \Theta + \Delta_{\text{aw}}^H)^H \\
&+ 2\Re \left\{ (\Delta_{\text{rw}}^H \Theta \mathbf{G} + \Delta_{\text{aw}}^H) \mathbf{R} (\hat{\mathbf{h}}_{\text{aw}}^H + \hat{\mathbf{h}}_{\text{rw}}^H \Theta \mathbf{G})^H \right\} \\
&+ (\hat{\mathbf{h}}_{\text{aw}}^H + \hat{\mathbf{h}}_{\text{rw}}^H \Theta \mathbf{G}) \mathbf{R} (\hat{\mathbf{h}}_{\text{aw}}^H + \hat{\mathbf{h}}_{\text{rw}}^H \Theta) \\
&= \bar{\Delta}_{\text{w}}^H \bar{\mathbf{G}} \bar{\mathbf{R}} \bar{\mathbf{G}}^H \bar{\Delta}_{\text{w}} + 2\Re \left\{ \bar{\Delta}_{\text{w}}^H \bar{\mathbf{G}} \bar{\mathbf{R}} \bar{\mathbf{G}}^H \bar{\mathbf{h}}_{\text{w}} \right\} + \bar{\mathbf{h}}_{\text{w}}^H \bar{\mathbf{G}} \bar{\mathbf{R}} \bar{\mathbf{G}}^H \bar{\mathbf{h}}_{\text{w}}, \quad (55)
\end{aligned}$$

where $\bar{\mathbf{G}} \triangleq [\mathbf{G}^H \Theta^H, \mathbf{I}_{N_A}]^H$, $\bar{\mathbf{h}}_{\text{w}}^H \triangleq [\hat{\mathbf{h}}_{\text{rw}}^H, \hat{\mathbf{h}}_{\text{aw}}^H]$ and $\bar{\Delta}_{\text{w}}^H \triangleq [\Delta_{\text{rw}}^H, \Delta_{\text{aw}}^H]$.

According to (29), we have

$$\bar{\Delta}_{\text{w}}^H \mathbf{P}_1 \bar{\Delta}_{\text{w}} - \delta_{\text{rw}}^2 \leq 0, \quad \bar{\Delta}_{\text{w}}^H \mathbf{P}_2 \bar{\Delta}_{\text{w}} - \delta_{\text{aw}}^2 \leq 0, \quad (56)$$

where $\mathbf{P}_1 = \text{blkdiag}(\mathbf{I}_{N_R}, \mathbf{0}_{N_A \times N_A})$ and $\mathbf{P}_2 = \text{blkdiag}(\mathbf{0}_{N_R \times N_R}, \mathbf{I}_{N_A})$. Then, by defining in (57) on the top of the next page and based on Lemma 1, we can obtain the LMI as follows

$$\sum_{i=1}^2 \mu_i \begin{bmatrix} \mathbf{P}_i & \mathbf{q}_i \\ \mathbf{q}_i^H & q_i \end{bmatrix} \succeq \begin{bmatrix} \mathbf{P}_0 & \mathbf{q}_0 \\ \mathbf{q}_0^H & q_0 \end{bmatrix} \Rightarrow \begin{bmatrix} \mathbf{P} + \boldsymbol{\mu} & \mathbf{q} \\ \mathbf{q}^H & q \end{bmatrix} \succeq \mathbf{0}, \quad (59)$$

where $\mathbf{P} = -\mathbf{P}_0$, $\boldsymbol{\mu} = \text{blkdiag}(\mu_1 \mathbf{I}_{N_R}, \mu_2 \mathbf{I}_{N_A})$, $\mathbf{q} = -\mathbf{q}_0$, $q = -q_0 - \mu_1 \delta_{\text{rw}}^2 - \mu_2 \delta_{\text{aw}}^2$, $\mu_1 \geq 0$ and $\mu_2 \geq 0$ are slack variables. The proof is thus completed. ■

APPENDIX B PROOF OF PROPOSITION 3

Problem $\bar{\mathcal{P}}2$ is jointly convex with respect to the optimization variables and satisfies Slater's constraint qualification. Therefore, strong duality holds, and the Lagrangian function in terms of \mathbf{W}_k is given by

$$\begin{aligned}
\mathcal{L} &= Q_1 - \sum_{k \in \mathcal{K}} \text{tr} \left(\nabla_{\mathbf{W}_k}^H P_1 \left(\mathbf{W}^{(m)}, \mathbf{R}_s^{(m)} \right) \mathbf{W}_k \right) \\
&- \gamma \sum_{k \in \mathcal{K}} \text{tr}(\mathbf{W}_k) + \sum_{k \in \mathcal{K}} \text{tr}(\boldsymbol{\Upsilon}_k \mathbf{W}_k) + \text{tr}(\boldsymbol{\Omega} \boldsymbol{\Pi}) + \xi, \quad (60)
\end{aligned}$$

where ξ includes all the terms that do not involve \mathbf{W}_k . Let $\gamma \geq 0$, $\boldsymbol{\Upsilon}_k \in \mathbb{H}^{N_A}$ and $\boldsymbol{\Xi} \in \mathbb{H}^{N_A + N_R + 1}$ denote the Lagrange multipliers associated with constraints $\bar{\mathcal{C}}1$, $\bar{\mathcal{C}}2$ and $\bar{\mathcal{C}}6$ in problem (43), respectively. Then, we investigate the structure of \mathbf{W}_k by checking the Karush-Kuhn-Tucker (KKT) conditions of problem, which are given by

$$\begin{aligned}
\text{K1} : \boldsymbol{\Upsilon}_k^* \mathbf{W}_k^* &= \mathbf{0}, \quad \text{K2} : \gamma^* \geq 0, \boldsymbol{\Upsilon}_k^* \succeq \mathbf{0}, \boldsymbol{\Omega}^* \succeq \mathbf{0}, \\
\text{K3} : \nabla_{\mathbf{W}_k} \mathcal{L}(\mathbf{W}_k^*) &= \mathbf{0} \quad (61)
\end{aligned}$$

where γ^* , $\boldsymbol{\Upsilon}_k^*$, and $\boldsymbol{\Omega}^*$ are the optimal Lagrangian multipliers. Based on K3, we have $\boldsymbol{\Upsilon}_k^* = \gamma^* \mathbf{I}_{N_A} - \boldsymbol{\Xi}_k^*$, where

$$\begin{aligned}
\boldsymbol{\Xi}_k^* &= \frac{1}{\ln 2} \sum_{j \in \mathcal{K}} \frac{\mathbf{h}_j \mathbf{h}_j^H}{\text{tr}(\mathbf{h}_j \mathbf{h}_j^H \mathbf{R}_s) + \sum_{i \in \mathcal{K}} \text{tr}(\mathbf{h}_j \mathbf{h}_j^H \mathbf{W}_i) + \sigma_{b,j}^2} \\
&- \nabla_{\mathbf{W}_k} P_1 \left(\mathbf{W}^{(m)}, \mathbf{R}_s^{(m)} \right) + \nabla_{\mathbf{W}_k} \text{tr}(\boldsymbol{\Omega}^* \boldsymbol{\Pi}). \quad (62)
\end{aligned}$$

According to $\boldsymbol{\Upsilon}_k^* \succeq \mathbf{0}$ in K2, $\gamma^* \geq \lambda_{\max}(\boldsymbol{\Xi}_k^*)$ must hold. Then, we have the following conclusions:

- $\gamma^* > \lambda_{\max}(\boldsymbol{\Xi}_k^*)$: it will result in a positive definite and full-rank matrix $\boldsymbol{\Upsilon}_k^* \succ \mathbf{0}$. Based on K1, we have $\mathbf{W}_k = \mathbf{0}$, which is obviously not a feasible solution of problem $\bar{\mathcal{P}}2$.
- $\gamma^* = \lambda_{\max}(\boldsymbol{\Xi}_k^*)$: in this case, we have $N_A - 1 \leq \text{rank}(\boldsymbol{\Upsilon}_k^*) < N_A$, then according to K1 and the Sylvester inequality, we have $N_A - 1 + \text{rank}(\mathbf{W}_k^*) \leq \text{rank}(\boldsymbol{\Upsilon}_k^*) + \text{rank}(\mathbf{W}_k^*) \leq N_A \Rightarrow \text{rank}(\mathbf{W}_k^*) \leq 1$.

Based on the above derivation, $\text{rank}(\mathbf{W}_k^*) \leq 1$ follows. ■

APPENDIX C PROOF OF PROPOSITION 4

We first perform the singular value decomposition (SVD) of $\mathbf{R} = \sum_i \mathbf{p}_i \mathbf{q}_i^H$ in Proposition 2 and then define that

$$\begin{aligned}
\bar{\mathbf{P}}_i &= \begin{bmatrix} \text{diag}(\mathbf{G} \mathbf{p}_i) & \mathbf{0}_{N_R \times 1} \\ \mathbf{0}_{N_A \times N_R} & \mathbf{p}_i \end{bmatrix}, \\
\bar{\mathbf{Q}}_i &= \begin{bmatrix} \text{diag}(\mathbf{q}_i^H \mathbf{G}^H) & \mathbf{0}_{N_R \times N_A} \\ \mathbf{0}_{1 \times N_R} & \mathbf{q}_i^H \end{bmatrix}. \quad (63)
\end{aligned}$$

$$\mathbf{P}_0 = \bar{\mathbf{G}}\mathbf{R}\bar{\mathbf{G}}^H, \mathbf{q}_0 = \mathbf{P}_0\bar{\mathbf{h}}_w, q_0 = \bar{\mathbf{h}}_w^H \mathbf{P}_0 \bar{\mathbf{h}}_w - (\eta_2 - 1)\sigma_w^2, \mathbf{x} = \bar{\Delta}_w, \mathbf{q}_1 = \mathbf{q}_2 = \mathbf{0}_{(N_A+N_R)\times 1}, q_1 = -\delta_{\text{rw}}^2, q_2 = -\delta_{\text{aw}}^2. \quad (57)$$

$$\hat{\mathbf{P}} = -\sum_i \bar{\mathbf{P}}_i \mathbf{V}^* \bar{\mathbf{Q}}_i, \hat{\mathbf{q}} = \hat{\mathbf{P}}\bar{\mathbf{h}}_w, \hat{\boldsymbol{\mu}} = \text{blkdiag}(\hat{\mu}_1 \mathbf{I}_{N_R}, \hat{\mu}_2 \mathbf{I}_{N_A}), \hat{\mathbf{q}} = \bar{\mathbf{h}}_w^H \hat{\mathbf{P}} \bar{\mathbf{h}}_w + (\eta_2 - 1)\sigma_w^2 - \hat{\mu}_1 \delta_{\text{rw}}^2 - \hat{\mu}_2 \delta_{\text{aw}}^2. \quad (58)$$

According to (55), we can rewrite $\bar{\mathbf{G}}\mathbf{R}\bar{\mathbf{G}}^H$ as follows

$$\begin{aligned} \bar{\mathbf{G}}\mathbf{R}\bar{\mathbf{G}}^H &= \sum_i \begin{bmatrix} \boldsymbol{\Theta} \mathbf{G} \mathbf{p}_i \mathbf{q}_i^H \mathbf{G}^H \boldsymbol{\Theta}^H & \boldsymbol{\Theta} \mathbf{G} \mathbf{p}_i \mathbf{q}_i^H \\ \mathbf{p}_i \mathbf{q}_i^H \mathbf{G}^H \boldsymbol{\Theta}^H & \mathbf{p}_i \mathbf{q}_i^H \end{bmatrix} \\ &= \sum_i \begin{bmatrix} \text{diag}(\mathbf{G} \mathbf{p}_i) \boldsymbol{\theta} \boldsymbol{\theta}^H \text{diag}(\mathbf{q}_i^H \mathbf{G}^H) & \text{diag}(\mathbf{G} \mathbf{p}_i) \boldsymbol{\theta} \mathbf{q}_i^H \\ \mathbf{p}_i \boldsymbol{\theta}^H \text{diag}(\mathbf{q}_i^H \mathbf{G}^H) & \mathbf{p}_i \mathbf{q}_i^H \end{bmatrix} \\ &= \sum_i \bar{\mathbf{P}}_i \mathbf{V}^* \bar{\mathbf{Q}}_i. \end{aligned} \quad (64)$$

Hence, similar to Proposition 2, and based on the definition in (58) on the top of next page, the covertness constraint in (44) can be equivalently transformed into

$$\begin{bmatrix} \hat{\mathbf{P}} + \hat{\boldsymbol{\mu}} & \hat{\mathbf{q}} \\ \hat{\mathbf{q}}^H & \hat{\mathbf{q}} \end{bmatrix} \succeq \mathbf{0}, \quad (65)$$

where $\hat{\mu}_1 \geq 0$ and $\hat{\mu}_2 \geq 0$ are slack variables. This completes the proof. ■

REFERENCES

- [1] X. Chen *et al.*, "Covert communications: A comprehensive survey," *IEEE Commun. Surveys Tuts.*, vol. 25, no. 2, pp. 1173–1198, 2nd Quart., Apr. 2023.
- [2] X. Yuan, Y.-J. A. Zhang, Y. Shi, W. Yan, and H. Liu, "Reconfigurable-intelligent-surface empowered wireless communications: Challenges and opportunities," *IEEE Wireless Commun.*, vol. 28, no. 2, pp. 136–143, Apr. 2021.
- [3] S. Ma, Y. Zhang, H. Li, S. Lu, N. Al-Dhahir, S. Zhang, and S. Li, "Robust beamforming design for covert communications," *IEEE Trans. Inf. Forensics Security.*, vol. 16, pp. 3026–3038, 2021.
- [4] O. Shmuel, A. Cohen, and O. Gurewitz, "Multi-antenna jamming in covert communication," *IEEE Trans. Commun.*, vol. 69, no. 7, pp. 4644–4658, Jul. 2021.
- [5] S. Ma *et al.*, "Covert beamforming design for Intelligent-Reflecting-Surface-assisted IoT networks," *IEEE Internet Things J.*, vol. 9, no. 7, pp. 5489–5501, Apr. 2022.
- [6] X. Zhou, S. Yan, Q. Wu, F. Shu, and D. W. K. Ng, "Intelligent reflecting surface (IRS)-aided covert wireless communications with delay constraint," *IEEE Trans. Wireless Commun.*, vol. 21, no. 1, pp. 532–547, Jan. 2021.
- [7] C. Wang, Z. Li, J. Shi, and D. W. K. Ng, "Intelligent reflecting surface-assisted multi-antenna covert communications: Joint active and passive beamforming optimization," *IEEE Trans. Commun.*, vol. 69, no. 6, pp. 3984–4000, Jun. 2021.
- [8] J. Si, Z. Li, Y. Zhao, J. Cheng, L. Guan, J. Shi, and N. Al-Dhahir, "Covert transmission assisted by intelligent reflecting surface," *IEEE Trans. Commun.*, vol. 69, no. 8, pp. 5394–5408, Aug. 2021.
- [9] S. Ma *et al.*, "Covert beamforming design for integrated radar sensing and communication systems," *IEEE Trans. Wireless Commun.*, vol. 22, no. 1, pp. 718–731, Jan. 2023.
- [10] J. Hu, Q. Lin, S. Yan, X. Zhou, Y. Chen, and F. Shu, "Covert transmission via integrated sensing and communication systems," *IEEE Trans. Veh. Technol.*, vol. 73, no. 3, pp. 4441–4446, Mar. 2024.
- [11] L. Hu, R. Yang, L. Wu, C. Huang, Y. Jiang, L. Chen, and X. Zhou, "RIS-assisted integrated sensing and covert communication design," *IEEE Internet Things J.*, vol. 11, no. 9, pp. 16 505–16 516, May. 2024.
- [12] A. Liu *et al.*, "A survey on fundamental limits of integrated sensing and communication," *IEEE Commun. Surveys Tuts.*, vol. 24, no. 2, pp. 994–1034, Feb. 2022.
- [13] J. A. Zhang *et al.*, "Enabling joint communication and radar sensing in mobile networks—A survey," *IEEE Commun. Surveys Tuts.*, vol. 24, no. 1, pp. 306–345, 1st Quart., 2022.
- [14] H. Du, J. Kang, D. Niyato, J. Zhang, and D. I. Kim, "Reconfigurable intelligent surface-aided joint radar and covert communications: Fundamentals, optimization, and challenges," *IEEE Veh. Technol. Mag.*, vol. 17, no. 3, pp. 54–64, Sep. 2022.
- [15] Y. Zhang, W. Ni, J. Wang, W. Tang, M. Jia, Y. C. Eldar, and D. Niyato, "Robust transceiver design for covert integrated sensing and communications with imperfect CSI," *IEEE Trans. Commun.*, early access, 2024.
- [16] X. Zhao, W. Deng, M. Li, and M.-J. Zhao, "Robust beamforming design for integrated sensing and covert communication systems," *IEEE Wireless Commun. Lett.*, vol. 13, no. 9, pp. 2566–2570, Sep. 2024.
- [17] Z. Wei, F. Liu, C. Liu, Z. Yang, D. W. K. Ng, and R. Schober, "Integrated sensing, navigation, and communication for secure UAV networks with a mobile eavesdropper," *IEEE Trans. Wireless Commun.*, vol. 23, no. 7, pp. 7060–7078, Jul. 2024.
- [18] X. Wang, Z. Fei, P. Liu, J. A. Zhang, Q. Wu, and N. Wu, "Sensing aided covert communications: Turning interference into Allies," *IEEE Trans. Wireless Commun.*, early access, 2024.
- [19] C. Ruan, Z. Zhang, H. Jiang, J. Dang, L. Wu, and H. Zhang, "Approximate message passing for channel estimation in reconfigurable intelligent surface aided MIMO multiuser systems," *IEEE Trans. Commun.*, vol. 70, no. 8, pp. 5469–5481, Aug. 2022.
- [20] G. Zhou, C. Pan, H. Ren, P. Popovski, and A. L. Swindlehurst, "Channel estimation for ris-aided multiuser millimeter-wave systems," *IEEE Trans. Signal Process.*, vol. 70, pp. 1478–1492, 2022.
- [21] M. Luan, B. Wang, Z. Chang, T. Hämäläinen, and F. Hu, "Robust beamforming design for RIS-aided integrated sensing and communication system," *IEEE Trans. Intell. Transp. Syst.*, vol. 24, no. 6, pp. 6227–6243, Jun. 2023.
- [22] P. Liu, Z. Fei, X. Wang, J. A. Zhang, Z. Zheng, and Q. Zhang, "Securing multi-user uplink communications against mobile aerial eavesdropper via sensing," *IEEE Trans. Veh. Technol.*, vol. 72, no. 7, pp. 9608–9613, Jul. 2023.
- [23] Y. Zeng, Q. Wu, and R. Zhang, "Accessing from the sky: A tutorial on UAV communications for 5G and beyond," *Proc. IEEE*, vol. 107, no. 12, pp. 2327–2375, Dec. 2019.
- [24] F. Liu, W. Yuan, C. Masouros, and J. Yuan, "Radar-assisted predictive beamforming for vehicular links: Communication served by sensing," *IEEE Trans. Wireless Commun.*, vol. 19, no. 11, pp. 7704–7719, Nov. 2020.
- [25] S. M. Kay, *Fundamentals of Statistical Signal Processing: Estimation Theory*. Prentice-Hall, Inc., 1993.
- [26] T. Bai, J. Wang, Y. Ren, and L. Hanzo, "Energy-efficient computation offloading for secure UAV-edge-computing systems," *IEEE Trans. Veh. Technol.*, vol. 68, no. 6, pp. 6074–6087, Jun. 2019.
- [27] C. Han, L. Bai, T. Bai, and J. Choi, "Joint UAV deployment and power allocation for secure space-air-ground communications," *IEEE Trans. Commun.*, vol. 70, no. 10, pp. 6804–6818, Oct. 2022.
- [28] B. Li, Z. Fei, Y. Zhang, and M. Guizani, "Secure UAV communication networks over 5G," *IEEE Wireless Commun.*, vol. 26, no. 5, pp. 114–120, Oct. 2019.
- [29] J. Zhang, M. Li, M.-J. Zhao, X. Ji, and W. Xu, "Multi-user beam training and transmission design for covert millimeter-wave communication," *IEEE Trans. Inf. Forensics Security.*, vol. 17, pp. 1528–1543, Mar. 2022.
- [30] T. M. Cover, *Elements of information theory*. John Wiley & Sons, 1999.
- [31] Z. Wei, F. Liu, D. W. K. Ng, and R. Schober, "Safeguarding uav networks through integrated sensing, jamming, and communications," in *ICASSP 2022 - 2022 IEEE International Conference on Acoustics, Speech and Signal Processing (ICASSP)*. IEEE, 2022, pp. 8737–8741.
- [32] S. Boyd, L. E. Ghaoui, E. Feron, and V. Balakrishnan, *Linear Matrix Inequality in Systems and Control Theory*. Philadelphia, PA, USA: SIAM, 1994.
- [33] M. Grant *et al.*, "CVX: Matlab software for disciplined convex programming, version 2.1." [Online]. Available: <http://cvxr.com/cvx>
- [34] P. Cao, J. Thompson, and H. V. Poor, "A sequential constraint relaxation algorithm for rank-one constrained problems," in *Proc. 25th Eur. Signal Process. Conf. (EUSIPCO)*, Aug. 2017, pp. 1060–1064.
- [35] X. Zhang, *Matrix Analysis and Applications*. China: Tsinghua Univ. Press, 2013.
- [36] Y. Sun, P. Babu, and D. P. Palomar, "Majorization-minimization algorithms in signal processing, communications, and machine learning," *IEEE Trans. Signal Process.*, vol. 65, no. 3, pp. 794–816, Feb. 2016.
- [37] G. Zhou, C. Pan, H. Ren, K. Wang, and A. Nallanathan, "A framework of robust transmission design for IRS-aided MISO communications with imperfect cascaded channels," *IEEE Trans. Signal Process.*, vol. 68, pp. 5092–5106, Jan. 2020.
- [38] X. Yu, D. Xu, Y. Sun, D. W. K. Ng, and R. Schober, "Robust and secure wireless communications via intelligent reflecting surfaces," *IEEE J. Sel. Areas Commun.*, vol. 38, no. 11, pp. 2637–2652, Jul. 2020.